Anharmonic adlayer vibrations on the Si(111):H surface

R. Honke
Institut für Theoretische Physik, Universität Regensburg, D-93040 Regensburg, Germany

P. Jakob* and Y. J. Chabal
Bell Laboratories, Lucent Technologies, 600 Mountain Avenue, Murray Hill, New Jersey 07974

A. Dvořák, S. Tausendpfund, W. Stigler, P. Pavone, A. P. Mayer, and U. Schröder
Institut für Theoretische Physik, Universität Regensburg, D-93040 Regensburg, Germany
(Received 11 September 1998)

Using infrared absorption spectroscopy, the frequency and linewidth of the H-stretching vibration on the Si(111):H-(1×1) surface has been measured over a temperature range of 14–350 K. An *ab initio* calculation of the temperature dependence of the anharmonic frequency shift and the intrinsic linewidth of this mode has been carried out, which fully accounts for the quantum nature of the atomic vibrations by using interacting phonon theory. The theoretical results show that at temperatures greater than 200 K, both line shift and linewidth of the stretching mode are primarily due to strong anharmonic coupling to the bending modes, which suffer decay into substrate modes via cubic anharmonicity. At low temperatures, direct coupling to various phonon modes of the substrate dominates the temperature dependence of the line shift. In addition, predictions are made for the frequency shift due to zero-point motion of the atoms. A strong sensitivity of the frequency on the shape of the Si-H potential has been found that makes quantitative predictions of the influence of zero-point motion very difficult. As a byproduct, the temperature dependence of the interatomic distances near the surface has been obtained and a decrease of the H-Si distance with increasing temperature is predicted. [S0163-1829(99)02016-0]

I. INTRODUCTION

The physical properties of low-index surfaces of silicon crystals have been extensively studied in recent years.[1] Among them, the Si(111) surface has probably received more attention than any other semiconductor surface. The strongly covalent character of the silicon-silicon bonds leads to the well-known reconstruction patterns of these surfaces. The advent of wet chemical preparation techniques[2–4] made it possible to generate silicon surfaces covered with one monolayer of hydrogen.[5] The hydrogen atoms saturate the dangling bonds giving rise to a surface structure that is almost ideal in the sense that the silicon atoms near the surface take almost the positions that would correspond to their bulk equilibrium positions.

In addition to basic scientific interests, there is also a technological motivation for studying the structure as well as the dynamics of hydrogenated silicon surfaces. Electronic processes occurring at the surfaces of semiconductor devices sometimes involve surface and adsorbate phonon modes and their relaxation into substrate phonons.[6]

Dynamical properties of the Si(111):H surface have been studied by helium atom scattering,[7,8] high-resolution electron energy loss spectroscopy,[9,10] and infrared absorption spectroscopy[2,11–13] and sum frequency generation.[14–17] The structure and the lattice vibrations of the system Si(111):H-(1×1) have been investigated theoretically by model calculations[7,18] (the second one without hydrogen termination), by semiempirical approaches[19,20] and by *ab initio* methods.[21–27] Some of these works investigated the vibrations of the hydrogen atoms on a rigid silicon substrate by a frozen phonon calculation.[22,23] Others used molecular dynamics within a semiempirical tight-binding approach[19,28] or with first-principles forces on the basis of the Car-Parinnello method.[24,26] Full phonon dispersion curves along symmetry directions in the surface Brillouin zone have been determined using lattice-dynamical models,[7,18] a semiempirical tight-binding approach[20] and *ab initio* using density-functional perturbation theory.[27] The phonon modes of the hydrogen-covered (111) surface of a silicon substrate can be grouped into bulk and surface modes of the substrate material, which have been determined theoretically in very good agreement with experimental data, and into adsorbate vibrations, namely, the hydrogen stretching and bending modes. The hydrogen stretching mode has a frequency of more than four times the maximum frequency of the silicon phonon modes. While this frequency is known experimentally to a very high precision, the corresponding theoretical values found in the literature scatter considerably. One goal of this paper is to clarify the reasons for these discrepancies and especially to assess the role of anharmonicity.

Beyond phonon frequencies and associated displacement characteristics, which in most cases may be described within the harmonic approximation with possible anharmonic corrections, several experiments in the past have focused directly on anharmonic properties of the adlayer modes.[2,14,15] The H/Si(111) surface is very suitable for the study of such properties because the electronic gap is much larger than the Si-H stretch vibrations considered here and the inhomogeneous broadening[29,30] ($\approx 0.05\,\mathrm{cm}^{-1}$) is much smaller than in other systems. The lifetime broadening is due only to multiphonon relaxation and has been measured directly by time-

resolved spectroscopy.[16,31,32] On flat Si(111), the monohydride relaxes extremely slowly ($\approx$ 1 nsec) contributing less than $0.01\,\mathrm{cm}^{-1}$ to the linewidth.

In particular, the temperature dependences of the Si-H stretch mode line position and linewidth has been measured by infrared absorption.[2] While in these earlier measurements an extrapolation of the frequency to 0 K was difficult, frequency data have been taken over a much larger temperature range down to much lower temperatures in the present work. Our new experimental results suggest that the anharmonic coupling between the adsorbate modes and vibrational modes of the silicon substrate is paramount for a proper description of the temperature dependence of the stretching mode frequency and its intrinsic linewidth. The contribution of zero-point motion to this frequency and its temperature dependence are calculated, using an *ab initio* technique that is free of any model parameters. Thereby the phonon modes responsible for the temperature dependence of the stretching mode frequency are identified.

The paper is organized in the following way: In the next section, the preparation of the Si(111):H surface and the experimental setup are briefly described, and infrared data for temperatures between 14 and 350 K are presented. In the subsequent section, the structure of the system and the phonon spectrum, obtained within the harmonic approximation, are discussed. Here, we also give some technical details concerning our *ab initio* calculations. The fourth section is devoted to the anharmonic dynamics of the hydrogen atoms in the rigid substrate approximation, i.e., with the silicon atoms kept fixed at their classical equilibrium positions. The infrared absorption spectrum of the system is calculated within this approximation, the appearance of multiphonon bound states is discussed, and the connection with intrinsic localized modes or discrete breathers,[33,34] a much discussed phenomenon of classical nonlinear dynamics, is established. In Sec. V, the coupling of the adsorbate modes to the substrate modes is taken into account. Particular attention is paid to the anharmonic shifts of the atomic equilibrium positions near the surface as they enter the calculations of the frequency shift in a sensitive manner. Our theoretical results for the temperature dependence of the anharmonic line shift and the linewidth of the stretching mode in the infrared absorption spectrum are discussed and compared to the experimental data of Sec. II. The paper ends with a final discussion and some conclusions.

II. EXPERIMENT

There are three important aspects of the experiment: the wet chemical preparation of the flat H/Si(111), the ability to mount, cool, and measure the sample in an ultrahigh vacuum environment, and the high resolution of the IR spectrometer. To achieve the best surfaces, a thick thermal oxide is grown on the Si sample, prior to the chemical preparation. The sample is then thoroughly cleaned using the RCA steps for Si-Wafer cleaning,[35,36] before the thick oxide is etched in concentrated HF. The key step is the use of 40% ammonium fluoride solution immediately after to remove atomic roughness from the already H-terminated surface. The best results were obtained for a 3 1/2 min immersion in NH_4F at room temperature as characterized by infrared absorption spectroscopy. The UHV chamber is equipped with a load-lock system, through which the sample is introduced. To achieve the lowest temperatures ($\approx$14 K), the bevelled sample is mounted onto a Cu holder with a Cu front shield, with the only exposed part of the sample being the bevels at each end. The mounted samples are then introduced into the UHV part of the chamber. The temperature is measured in two ways: with a chromel/alumel thermocouple and with a Si diode (accuracy $\pm$1 K below 100 K) both attached to the Cu block. The temperature is varied by physically decoupling the sample holder block from the liquid-He reservoir. A high spectral resolution is critical to this experiment since the line can narrow to as low as $0.05\,\mathrm{cm}^{-1}$. The nominal resolution of the interferometer is $0.06\,\mathrm{cm}^{-1}$. The actual resolution is measured, using a CO cell and boxcar apodization, to be $0.04\,\mathrm{cm}^{-1}$. Two or four times zero filling is applied to obtain smooth line shapes. The detector is a liquid N_2-cooled InSb. No reference surface is necessary because the measured vibrational features are much sharper than any fluctuation or oscillation in the spectrum over the range of Si-H stretch vibrations ($2060-2150\,\mathrm{cm}^{-1}$), where a linear background is used.

The line shape of a vibrational mode primarily is characterized by a center frequency (ω) and a linewidth (Γ). Since anharmonic coupling induces a temperature dependence of both quantities, we performed experiments measuring $\omega(T)$ and $\Gamma(T)$ as a function of surface temperature. Figure 1 shows vibrational spectra of the $\nu_{\mathrm{Si\text{-}H}}$ mode taken at 294 and at 14 K. A marked red shift and line broadening of $\nu_{\mathrm{Si\text{-}H}}$ is found with increasing T. The data taken at very low temperatures ($T<50$ K) can be used to quantify line broadening mechanisms other than the dephasing process and to determine the line position in the absence of anharmonic coupling to thermal fluctuations; it is found that for the samples used in this work the $\nu_{\mathrm{Si\text{-}H}}$ line shape at low T is very close to being Lorentzian and $\omega(T)$ as well as $\Gamma(T)$ converge towards the zero K values of $\omega(0)=2085.99\,\mathrm{cm}^{-1}$ and $\Gamma(0)=0.08\,\mathrm{cm}^{-1}$, respectively. These numbers are crucial in the analysis of the data. The early fits of Dumas , Chabal, and Higashi,[2] used $\omega(0)=2086.25\,\mathrm{cm}^{-1}$, which they extrapolated from their lowest T spectra taken at 140 K. The better estimate of $\omega(0)$ in our work is made possible by the extension to lower temperatures (14 K). Also, the present data are obtained with much better spectral resolution ($0.04\,\mathrm{cm}^{-1}$ versus $0.3\,\mathrm{cm}^{-1}$) on samples with substantially better homogeneity than originally measured in Ref. 2: we measure a full width at half-maximum (FWHM) of $0.71\,\mathrm{cm}^{-1}$ instead of $0.85\,\mathrm{cm}^{-1}$ at 295 K, and of $0.08\,\mathrm{cm}^{-1}$ instead of an extrapolated value of $0.2\,\mathrm{cm}^{-1}$ at low temperatures. Note, however, that samples of different quality show the same temperature dependence of the Si-H stretch peak position, with however different absolute frequency position, due to average domain size: The larger the average domain size, the higher the Si-H stretch frequency.[29,37] These differences, in particular the discrepancy of $\omega(0)$,[38] are probably the main reasons for the extraction of a too low phonon frequency responsible for the dephasing process in Ref. 2.

There are two common ways to plot the data: a linear plot of ω and Γ as a function of temperature highlights the high temperature behavior while a logarithmic plot of $\Delta\omega(T) \equiv \omega(T)-\omega(0)$ and Γ versus the inverse temperature ($1/T$)

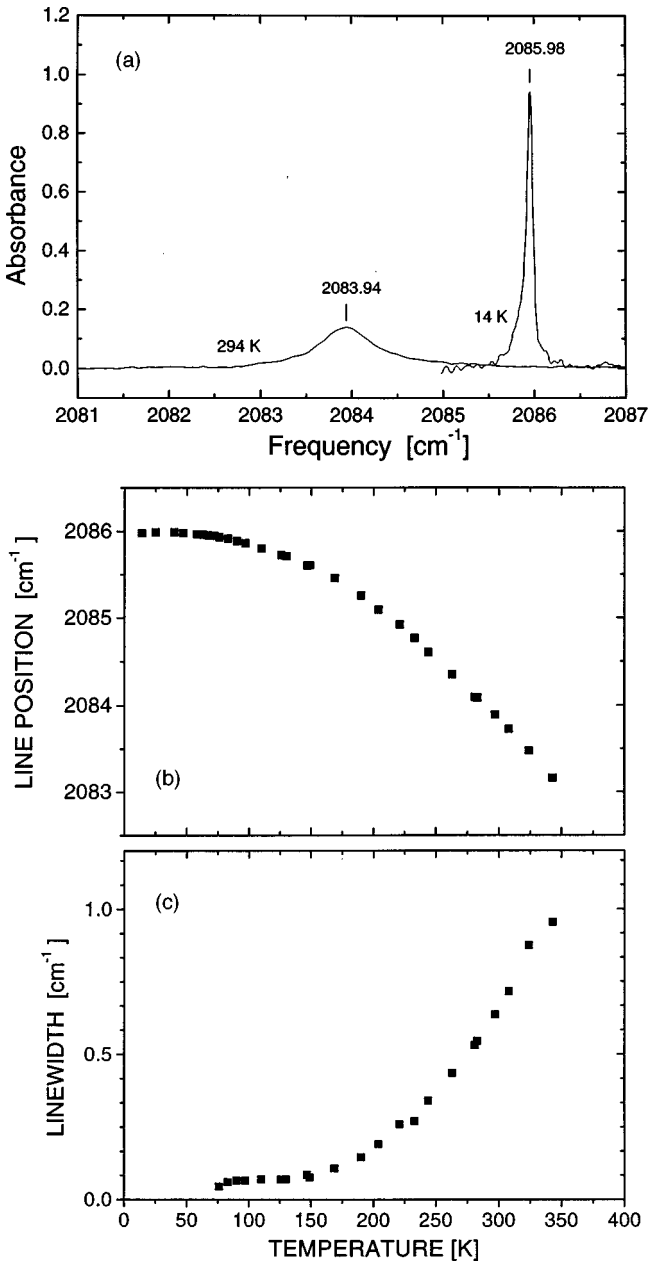

FIG. 1. (a) Set of infrared absorption spectra showing the Si-H stretch mode taken at room temperature ($T=294$ K) and at 14 K using a nominal spectral resolution of 0.12 and 0.06 cm^{-1}, respectively. The temperature dependent line position and linewidth of the Si-H stretch mode are displayed in (b) and (c).

emphasizes the low temperature behavior. The dependence at low temperatures is dominated by anharmonic coupling to low frequency phonons, while the high temperature data are sensitive to all phonon frequencies. Both types of plots are therefore commonly used.

Figures 1(b) and 1(c) show the linear dependence of $\omega(T)$ [Fig. 1(b)] and $\Gamma(T)$ [Fig. 1(c)] versus the temperature (the logarithmic dependence of $\Delta\omega(T)$ and $\Gamma(T)$ versus $1/T$, for H/Si(111)-(1×1) is presented below (Figs. 13 and 15), along with the results of our theoretical calculation). The data are obtained by a Lorentzian fit and a deconvolution of the inhomogeneous broadening using the lowest-temperature data ($T=14$ K).[39]

At temperatures below 140 K a puzzling observation is made: the width [Fig. 1(c)] levels off faster than expected and decreases only very slowly towards lower T. This is a minor effect, of order 0.05 cm^{-1}, but it unfortunately prevents an effective use of the low-T data.[40] Also a slight extra redshift of $\nu_{\text{Si-H}}$ mode by approximately 0.01–0.02 cm^{-1} with decreasing T is discernible.

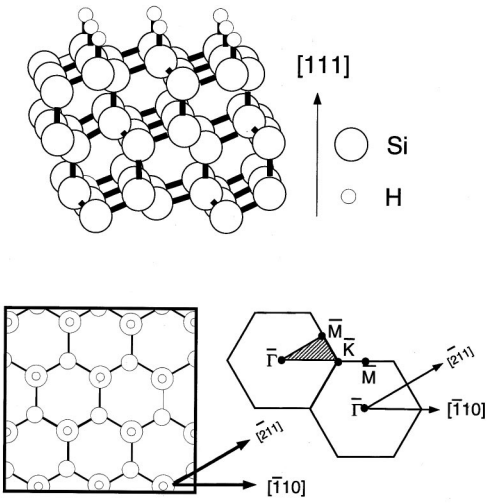

FIG. 2. Side view and top view of the hydrogenated Si(111) surface, and surface Brillouin zone.

III. STRUCTURE AND PHONON SPECTRUM IN THE HARMONIC APPROXIMATION

On the (111) surface of silicon, the hydrogen atoms form a triangular lattice as displayed in Fig. 2. They saturate the dangling bonds of the silicon atoms at the surface and hence no reconstruction occurs. In fact even at and near the surface, the silicon atoms take almost the same positions they would hold in a bulk crystal. This has been verified in our *ab initio* calculations, which have been carried out for a repeated slab geometry.[27,41] Each slab consists of 10 layers of silicon and both the top and bottom surface are covered with hydrogen. The vacuum distance between two adjacent slabs was chosen to be 8 Å. This distance was large enough that no dispersion was found for the electronic states along the direction normal to the surface. In the framework of the local-density approximation, the Kohn-Sham equations were solved in a plane-wave basis set. The interaction between the ions and valence electrons is described by soft nonlocal pseudopotentials of the Kerker[42] type for silicon and of the Troullier-Martins[43] type for hydrogen. A cutoff energy of 10 Ry was used with test calculations going up to 16 Ry. Integrations over electronic states in reciprocal space have been carried out at seven special points in the irreducible part of the surface Brillouin zone.[44] The atomic positions have been relaxed by finding the zeros of the Hellmann-Feynman forces.

Applying density-functional perturbation theory on the basis of the local density approximation,[45,46] phonon frequencies can be calculated for any wavevector in the surface Brillouin zone. In Fig. 3 the results of such a calculation are shown for the relaxed structure along the boundary of the irreducible wedge of the surface Brillouin zone as indicated in Fig. 2. They are compared with experimental data from high-resolution electron energy loss spectroscopy

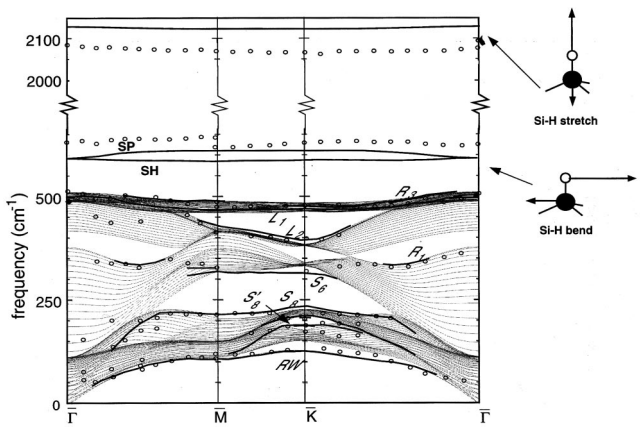

FIG. 3. Phonon dispersion along directions of high symmetry of the surface Brillouin zone. (Symmetric slab with 46 substrate layers.) Circles: HREELS data by Stuhlmann, Bogdány, and Ibach (Ref. 9). SH stands for shear-horizontal polarization and SP for polarization parallel to the wave vector. *RW* denotes the Rayleigh branch, L_1, L_2, S_6, S_8, and S_8' label various surface phonon branches, R_1 and R_3 denote surface resonances (Ref. 27).

(HREELS).[9] The phonon modes with frequencies below $500\,\mathrm{cm}^{-1}$ largely correspond to vibrations of the substrate atoms with the hydrogen following the motion of the underlying substrate atoms adiabatically. Only two surface branches (L_1,L_2) near the upper edge of the projected bulk phonon dispersion of silicon have eigenvectors with an appreciable contribution of hydrogen displacements.

Separated from the projected bulk spectrum of silicon there are three phonon branches that correspond to modes where mostly the hydrogen atoms are vibrating with only very small eigenvector components corresponding to the silicon atoms of the underlying substrate layers. At approximately $600\,\mathrm{cm}^{-1}$, two branches are located that correspond to two bending modes. The hydrogen atoms are vibrating parallel to the surface. At the $\bar{\Gamma}$ point, these two modes are degenerate, while at the $\bar{K}$ point, the two bending modes are not degenerate because of the lower symmetry of the substrate as compared to the triangular adsorbate lattice. The degeneracy is lifted even within the rigid-substrate approximation. The frequency splitting at the $\bar{M}$ point is found to be $24\,\mathrm{cm}^{-1}$ in good agreement with the HREELS value of $20\,\mathrm{cm}^{-1}$. In the rigid substrate approximation, when the silicon atoms are fixed at their equilibrium positions, the splitting at the $\bar{M}$ point reduces to $10\,\mathrm{cm}^{-1}$. The difference of $14\,\mathrm{cm}^{-1}$ reflects the fact that the eigenvectors of the bending modes have appreciable components corresponding to the displacements of the silicon atoms of the first layer. The remaining splitting and the remaining bandwidth of the bending mode branches may be due to dipole-dipole interaction of the hydrogen atoms as well as due to an indirect interaction via the electronic system in the substrate.

Far above the frequency region of the substrate modes, the branch of the hydrogen stretching vibrations is located at approximately $2100\,\mathrm{cm}^{-1}$. The total bandwidth of the stretching modes (including off-symmetry directions) was found to be around $9\,\mathrm{cm}^{-1}$ and the components in the associated eigenvectors corresponding to displacements of substrate atoms are very small. The dynamic dipole coupling

TABLE I. Hydrogen stretching mode frequency in the harmonic approximation. *R*, rigid substrate approximation; *a*, this work, 10 Ry cutoff, DFPT; *b*, this work, 30 Ry cutoff, molecular dynamics; *c*, this work, 10 Ry cutoff, frozen phonon. The experimental frequency at 0 K (differing from the harmonic value by anharmonic corrections) is $2086.0\,\mathrm{cm}^{-1}$ (see Fig. 1).

Frequency (cm^{-1})	Reference
2178	21 *R*
1997	22 *R*
2023	23 *R*
2022	25 *R*
2218	19
1984	24
1965	26
2071	20
2133	*a*
2104	*b*
2101	*c R*

approach applied to the stepped Si(111):H surface and extrapolated to large terrace sizes[12] yields a value of $\Delta\,\omega_{\mathrm{dyn}} = 7$–$8\,\mathrm{cm}^{-1}$ for the $\nu_{\mathrm{Si\text{-}H}}$ bandwidth in close agreement with the theoretical value.

While the phonon frequencies in the band of the substrate modes are in good agreement with experimental data, there are visible discrepancies for the bending and stretching vibrations. A comparison of our harmonic stretching and bending mode frequencies at the $\bar{\Gamma}$ point with experimental and other theoretical data is made in Table I.

One may be tempted to attribute these discrepancies to shortcomings of the *ab initio* methods used. In particular, the description of the interaction of the hydrogen ion with the valence electrons via a pseudopotential may appear unusual at first glance. Also, one may wonder whether the kinetic cutoff energy of 10 Ry used in most of our calculations has been sufficiently high to guarantee convergence. In order to test the latter point, the kinetic energy cutoff has been increased to 13 and 16 Ry. The values of the frequencies of the stretching and bending mode and the frequency of the Lucas modes at the Brillouin zone center and the silicon-hydrogen distance are shown in Table II for these three cases. The relative deviations from one cutoff value to the next is of the same order for the frequencies of the three modes. In order to provide an independent test of our *ab initio* scheme, we have also employed an alternative code[47] with a different pseudopotential generated by a scheme due to Hamann[48–50] and used in fully separable form.[51] The stretching mode frequency has been determined here by Car-Parinnello

TABLE II. Convergence behavior of phonon frequencies and the Si-H distance.

Cutoff energy (Ry)	10	13	16
$\nu_s\,(\mathrm{cm}^{-1})$	2133	2127	2144
$\nu_b\,(\mathrm{cm}^{-1})$	593	598	600
$\nu_{\mathrm{Lucas}}\,(\mathrm{cm}^{-1})$	493	498	499
$d_{\mathrm{Si\text{-}H}}$ (Å)	1.492	1.492	1.491

simulations.[47] These calculations have been carried out at a kinetic energy cutoff of 30 Ry, although tests for the silane molecule showed that they should have been converged at a lower cut-off. The resulting value for the stretching mode frequency of Si(111):H was $2104\,\mathrm{cm}^{-1}$. With this latter pseudopotential, it has also been possible to reproduce the experimental bond length and vibrational frequency of the hydrogen molecule[52] within 4% and 2%, respectively.

When assessing the remaining discrepancies between our theoretical values for the stretching mode frequency in the harmonic approximation, we have to note that these discrepancies are by orders of magnitude larger than the precision of $0.1\,\mathrm{cm}^{-1}$ that is reached in the infrared absorption spectroscopy (IRAS) experiments reported in Sec. II. However, we also stress that our theoretical values for the hydrogen stretching mode frequency are consistently higher than the experimental value. This fact will be explained through anharmonicity in the following section.

An approach going partly beyond the local-density approximation (LDA) is the generalized gradient approximation (GGA). A GGA implementation[53] is also provided in the code of the Fritz-Haber Institut.

A comparison of the hydrogen on-site potential for the two pseudopotential approaches based on the LDA and the one based on the generalized gradient approximation (GGA) (Ref. 53) is made in the next section, and very good agreement is found between them.

On the other hand, the strong zero-point motion of the hydrogen atoms is expected to cause non-negligible shifts to the bare (harmonic) frequencies of the adsorbate modes. This has partly served as a motivation to carry out the study reported on in this paper.

IV. RIGID SUBSTRATE APPROXIMATION

The primary goal of our theoretical analysis is to provide an understanding of the infrared absorption spectra of Si(111):H. In this system, infrared absorption is essentially due to the changes of the dipole moment through variations of the distance between the hydrogen atoms and the underlying silicon layer. These changes of the Si-H distance occur primarily in the hydrogen stretching vibrations which have eigenvectors with negligible content of substrate displacements. Therefore, the approximation of a rigid substrate with the silicon atoms kept fixed at their equilibrium positions should be a reasonable first approach for the description of the infrared absorption in this system. We may then start with the following Hamiltonian for the displacements $\mathbf{u}(l)$ of the hydrogen atoms from their classical equilibrium positions labelled by the index l:

$$H_{RS}=\sum_{l}\left\{\frac{\mathbf{p}^2(l)}{2m_H}+V(\mathbf{u}(l))\right\}+\frac{1}{2}\sum_{l,l'}\sum_{\alpha,\beta}\phi_{\alpha\beta}(ll')u_\alpha(l)u_\beta(l'),\qquad(1)$$

where m_H is the mass of a hydrogen atom and Greek indices denote Cartesian components. The terms in the curly brackets constitute the on-site Hamiltonian with the kinetic energy and with the on-site potential $V(\mathbf{u})$. Because of the small mass of the hydrogen atoms, their zero-point motion leads to large displacements. Therefore, the anharmonicity of the on-site potential is very important and will be fully taken into account. The last term in Eq. (1) is the intersite interaction. Its smallness is reflected in the small bandwidths of the stretching and bending mode dispersion curves. For a potential falling off as slowly as the $1/r$ Coulomb potential, anharmonic contributions to physical quantities come into play at first and higher orders of $\langle u^2\rangle/d_{\mathrm{H\text{-}H}}^2$, while the root mean square displacement $\sqrt{\langle u^2\rangle}$ of the hydrogen atoms is much smaller than the distance $d_{\mathrm{H\text{-}H}}$ between neighboring hydrogen atoms. Consequently, it suffices to account for the intersite interaction in harmonic approximation. In summary, we may characterize our system as *weakly coupled strongly anharmonic quantum oscillators*.

The on-site potential has been determined *ab initio* on a mesh of 2687 grid points by calculating the ground-state energy of the slab with the hydrogen film rigidly displaced. Kerker and Martins-Troullier pseudopotentials were used and a kinetic energy cutoff of 10 Ry. Figures 4(a) and 4(b) show the potentials for displacements in the direction normal to the surface *(z)* and along $(11\bar{2})$, i.e., the *x* direction, respectively. Obviously, the potential is very flat in the direction parallel to the surface. In order to test the precision of our numerical calculations of the on-site potential, we have repeated the calculations for the *z* and *x* directions shown in Fig. 4 with different pseudopotentials[48–51] as mentioned in the previous section and a cutoff of 30 Ry within LDA and GGA implemented in the code of the Fritz-Haber-Institut.[47,53] The results are practically identical with the data of the first calculation on the energy scale of Figs. 4(a), 4(b). They deviate only at large distances from the potential minimum.

The force constants $\phi_{\alpha\beta}(ll')$ for $l\neq l'$ are obtained from a calculation of dynamical matrices on the basis of density-functional perturbation theory (DFPT), and

$$\phi_{\alpha\beta}(ll)=-\sum_{l\neq l'}\phi_{\alpha\beta}(ll').\qquad(2)$$

The harmonic stretching and bending mode frequencies obtained from the above on-site potential by fitting to a parabola are $\omega_s=2101\,\mathrm{cm}^{-1}$ and $\omega_b=570\,\mathrm{cm}^{-1}$, which is 32 and $23\,\mathrm{cm}^{-1}$ lower than the harmonic frequency determined by DFPT in the full lattice-dynamical slab calculation.

In a first approximation, we neglect the intersite coupling. One may then try to determine the stretching and bending mode frequencies as an expansion in powers of $\hbar$. For this purpose, one has to expand the on-site potential $V(\mathbf{u})$ with respect to the displacement components.[23] The coefficients of this expansion have been obtained by differentiating numerically total energies, Hellmann-Feynman forces or second-order force constants determined by DFPT. At order $\hbar$, a frequency shift of about $100\,\mathrm{cm}^{-1}$ has been found for the stretching mode. Only cubic and quartic anharmonicity enter in this calculation. At order $\hbar^2$, fifth and sixth-order terms in the expansion of $V(\mathbf{u})$ are needed. They were found to contribute more than 50% of the $\hbar^2$ contribution. Its total value amounts to approximately $+37\,\mathrm{cm}^{-1}$. In the case of the bending mode, the contribution of order $\hbar^2$ is even larger than that of first order in $\hbar$ because of strong compensations between the perturbation-theoretical expressions. It is also

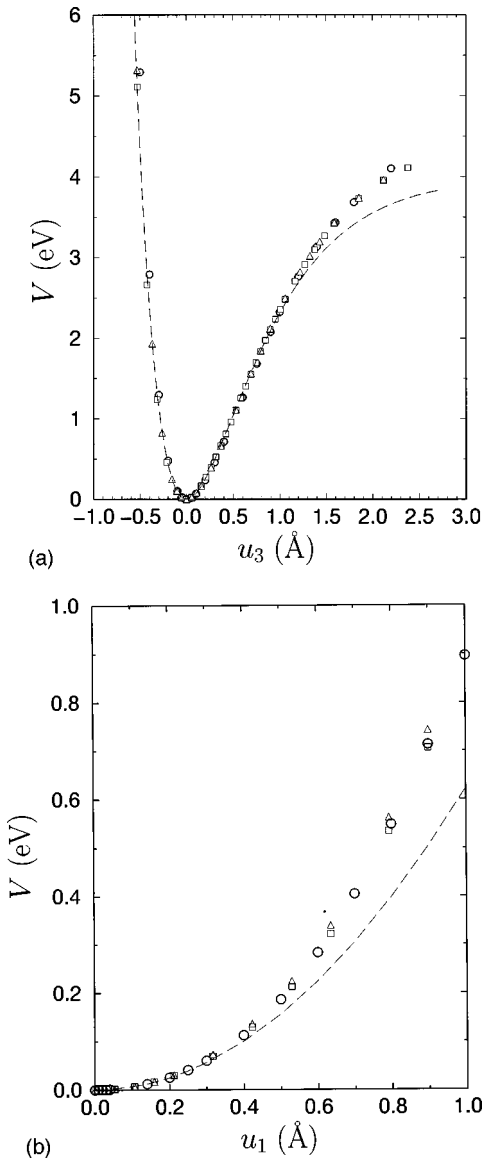

FIG. 4. On-site potential of the hydrogen atoms. (a) Potential along the surface normal. ○, LDA, 10 Ry cutoff, Kerker (H) and Troullier-Martins (Si) pseudopotentials; ◇, LDA, 30 Ry cutoff, Kleinman-Bylander separable pseudopotentials; △, GGA, 30 Ry cutoff, Kleinman-Bylander separable pseudopotentials; dashed line, Morse potential. (b) Potential along the *x* direction (parallel to the surface). ○, LDA, 10 Ry cutoff, Kerker (H) and Troullier-Martins (Si) pseudopotentials; ◇, LDA, 30 Ry cutoff, Kleinman-Bylander separable pseudopotentials; △, GGA, 30 Ry cutoff, Kleinman-Bylander separable pseudopotentials; dashed line, harmonic oscillator potential.

instructive to compare the relative magnitudes of the different terms in a diagrammatic representation of the contribution of order $\hbar^2$ to the anharmonic frequency shift and to the static displacement $\langle u_3\rangle$. It turns out that the contributions involving third-order static cumulants $\langle (u_\alpha - \langle u_\alpha\rangle)(u_\beta - \langle u_\beta\rangle)(u_\gamma - \langle u_\gamma\rangle)\rangle$ are not small. This indicates that self-consistent schemes which neglect these cumulants like the renormalized harmonic approximation in its simplest form do not seem to be appropriate for the system Si:H.

Therefore, as long as coupling to substrate modes is neglected, we go beyond low-order perturbation theory and diagonalize the full on-site Hamiltonian. For this purpose, we decompose the on-site potential in the following way:

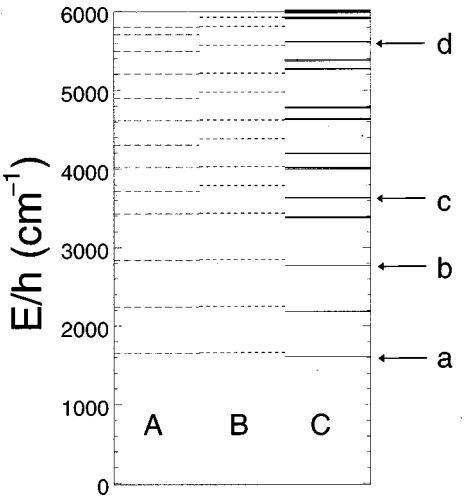

FIG. 5. Energy levels of the hydrogen on-site potential. *A*, Morse potential for displacements normal to the surface + two-dimensional (2D) harmonic oscillator for displacements parallel to the surface; *B*: anisotropic harmonic oscillator; *C*: complete on-site potential. (a) ground state; (b) second excited state of predominantly bending character; (c) first excited state of predominantly stretching character; (d) second excited state of predominantly stretching character.

$$V(\mathbf{u}) = D(1-e^{-\alpha u_3})^2 + \tfrac{1}{2} m_H \omega_b^2 (u_1^2+u_2^2) + W(\mathbf{u}), \quad (3)$$

where $\alpha^2 = m_H \omega_s^2/(2D)$ and the parameter D has been given the value 4 eV. ω_s and ω_b are the harmonic stretching and bending mode frequencies, respectively. Figure 4(a) shows that for $u_1 = u_2 = 0$, the on-site potential fits a Morse potential fairly well with the above values for α and D. On the observation that for distances of the order of the root mean square displacements of the hydrogen atoms due to their zero-point motion, $V(\mathbf{u})$ deviates very little from cylindrical symmetry around the u_3 axis, we let W depend only on the variables u_3 and $u_\parallel = \sqrt{u_1^2+u_2^2}$, putting $W(\mathbf{u}) \approx \tilde{W}(u_\parallel, u_3) = W(u_1,0,u_3)$. The eigenfunctions ψ_n^- of the full on-site Hamiltonian are then determined as linear combinations of products of eigenfunctions of the Morse Hamiltonian, $\varphi_{n_\perp}(u_3)$ with quantum number $n_\perp$, and the Hamiltonian of an isotropic two-dimensional harmonic oscillator, $\xi_{n_\parallel,m}(u_\parallel)\exp(im\phi)$ with radial quantum number $n_\parallel$ and angular quantum number m,

$$\psi_n^-(\mathbf{u}) = \sum_{n_\perp, n_\parallel, m} C^{(n)}_{n_\perp n_\parallel m}\, \varphi_{n_\perp}(u_3)\, \xi_{n_\parallel,m}(u_\parallel) e^{im\phi}, \quad (4)$$

where $\tan\phi = u_2/u_1$. The matrix elements of $\tilde{W}$ have been determined numerically, and the basis set of Morse and oscillator functions has been successively increased until convergence was reached for the eigenvalues E_n^-. The spectrum of eigenvalues determined in this way is shown in Fig. 5 and compared to the energy spectrum of a three-dimensional harmonic oscillator with frequencies $\omega_{s,b}$ and to the spectrum corresponding to the potential (3) with $W(\mathbf{u}) = 0$. [In all three cases, $V(0) = 0$.] Apart from a constant shift, the latter po-

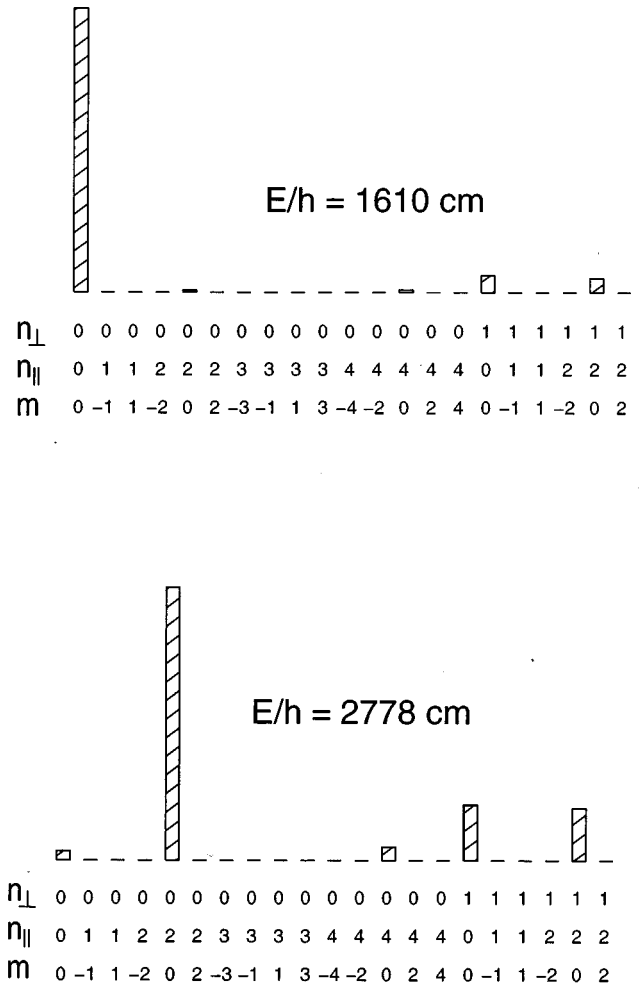

FIG. 6. Admixtures of basis states to the eigenstates with levels *a* and *b*. $n_\perp$, quantum number of the Morse potential; $n_\parallel, m$, radial and angular quantum numbers of the 2D isotropic harmonic oscillator potential.

tential reproduces the lowest six energy levels fairly well. However, strong deviations occur at higher energies.

An important feature of the additional potential W is that it couples the motion of the hydrogen atoms normal and parallel to the surface. This causes the eigenfunctions of predominant stretching character to contain appreciable admixtures of excited states of the bending motion and vice versa. Two examples are given in Fig. 6, where the modulus of the expansion coefficients $C^{(\bar{n})}_{n_\perp n_\parallel m}$ is plotted as a histogram over the quantum numbers $n_\perp, n_\parallel, m$, and it has important consequences on the infrared absorption spectrum.

A. Infrared absorption spectrum

In our system, infrared absorption happens essentially via the dipole moment normal to the surface, M_3, due to the presence of the hydrogen film. It may be expanded in powers of the hydrogen displacements:

$$M_3 = M_3^{(0)} + \sum_l \{M_{33}^{(1)} u_3(l) + \tfrac{1}{2} M_{333}^{(2)} u_3^2(l) + \tfrac{1}{2} M_{311}^{(2)} [u_1^2(l) + u_2^2(l)] + O(u^3)\}. \quad (5)$$

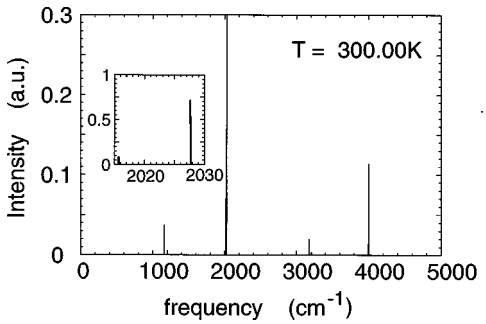

FIG. 7. Theoretical infrared absorption spectrum for decoupled hydrogen atoms on a rigid substrate.

Here u_3 denotes the displacement perpendicular to the surface (z). Second-order contributions involving two different lattice sites have been neglected in this expansion for the same reason we neglect the intersite interaction in comparison with the on-site potential.

The first-order dipole moment $M_{33}^{(1)}$ has been determined *ab initio* by differentiating numerically the dipole moment of a slab as a function of the distance between the hydrogen film and the substrate. Its value was found to be $1.3\,\mathrm{A\,s/m^2}$. In the same way, we have investigated the coefficients $M_{333}^{(2)}$ and $M_{311}^{(2)}$ and found them smaller than the accuracy of our numerical calculations. From these findings we conclude that the second-order infrared absorption from the hydrogen film should not exceed the background second-order absorption of the substrate, and it is essentially the first-order spectrum that is seen in the experiment. Having neglected intersite coupling, the absorbed intensity $I(\omega)$ is then proportional to the displacement-displacement correlation function of a single oscillator,

$$I(\omega) \propto \int_{-\infty}^{\infty} dt\, e^{i\omega t} \langle u_3(t) u_3(0) \rangle = \frac{2\pi\hbar}{Z} \sum_{m,n} e^{-\beta E_{\bar{n}}} |\langle \bar{n} | u_3 | \bar{m} \rangle|^2 \, \delta(\hbar\omega + E_{\bar{n}} - E_{\bar{m}}), \quad (6)$$

where $\beta = 1/(K_B T)$, T being the temperature and Z being the partition function of the anharmonic oscillator. The matrix elements $\langle \bar{n} | u_3 | \bar{m} \rangle$ have been determined numerically with the eigenfunctions introduced in the previous subsection.

In Fig. 7, the infrared spectrum is shown as obtained from an evaluation of expression (6) involving basis functions with $n_\parallel \leqslant 10$ and $n_\perp \leqslant 4$. In the harmonic approximation, the spectrum would consist of one peak only, situated at the bare stretching mode frequency ω_s. Because of the anharmonicity of the on-site potential of the hydrogen atoms, the following new features occur: (i) The position of the main peak is down-shifted by $71\,\mathrm{cm}^{-1}$. (ii) Additional lines appear at frequencies which are approximately higher harmonics of the frequency of the main peak, because the corresponding matrix elements of u_3 between the ground state and higher excited states no longer vanish. (iii) Small additional maxima appear around the strong peaks because the states of predominantly stretching character have energy levels that are no longer equidistant. (iv) As the on-site potential couples

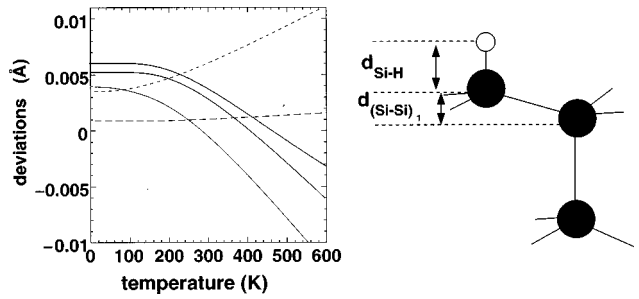

FIG. 8. Anharmonic shifts of interlayer distances. Solid lines, Si-H distance ($d_{\text{Si-H}} \approx 1.49$ Å); upper curve, exact result within rigid substrate approximation; center curve, first order perturbation theory without substrate modes; lower curve, first-order perturbation theory including substrate modes; dashed lines, distances between adjacent Si-Si layers; ($d_{\text{Si-Si}} \approx 0.77$ Å); upper curve, anharmonic shift of the distance between the first two substrate layers $d_{(\text{Si-Si})_1}$; lower curve: anharmonic shift of the distance between two corresponding substrate layers in the bulk $d_{(\text{Si-Si})_{bulk}}$.

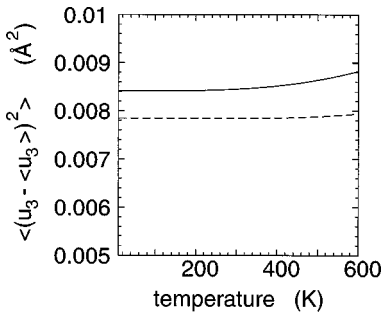

FIG. 9. Mean square displacements of the hydrogen atoms, rigid substrate approximation. Solid, anharmonic on-site potential; dashed, harmonic approximation.

displacements parallel and normal to the surface, the matrix element of u_3 between the ground state and the second of the excited states with predominantly bending character (see Fig. 6) is of considerable magnitude and gives rise to the lowest of the four major peaks in Fig. 7. The difference between the energies of the first excited state of predominantly bending nature and the ground state corresponds to $575\,\text{cm}^{-1}$, which is very close to the bare bending mode frequency of $570\,\text{cm}^{-1}$ in the rigid substrate approximation.

The spectrum at zero temperature looks very similar to the one at 300 K shown in Fig. 7 with the exception that the satellites near the four high peaks, which are due to transitions from thermally excited states, have disappeared and the high maxima themselves have slightly grown in intensity.

B. Mean positions and square displacements

By evaluating the moments

$$\langle (u_\alpha)^n \rangle = \frac{1}{Z} \sum_{\overline{m}} e^{-\beta E_{\overline{m}}} \langle \overline{m} | (u_\alpha)^n | \overline{m} \rangle \tag{7}$$

one obtains the contribution $\Delta d_{\text{Si-H}}$ of the zero-point and thermal motion of the hydrogen atoms to the Si-H distance ($n=1$, $\alpha=3$) and the mean square displacements ($n=2$) of the hydrogen atoms normal to the surface [Debye-Waller factor $W_\perp = \langle (u_3 - \langle u_3 \rangle)^2 \rangle$] and parallel to the surface ($W_\parallel = \langle u_1^2 \rangle$). The result for $\Delta d_{\text{Si-H}}$ is shown in Fig. 8 as the upper solid curve. The zero-point motion enlarges the Si-H distance by only 0.3%. With increasing temperature, this distance decreases. This behavior is due to the anharmonic coupling of the stretching mode to the bending vibrations. Taking into consideration that at temperatures below 600 K the bending modes, but not the stretching modes can be thermally excited and assuming that the bond length is conserved in the bending vibration, this decrease of $d_{\text{Si-H}}$ can be understood as a geometrical effect. On the whole, the anharmonic effects on the Si-H distance are surprisingly small. In fact, the root mean square displacement in the z direction ($\sqrt{W_\perp}$) is larger by almost a factor of 6. The temperature behavior of $W_\perp$ is shown in Fig. 9 and compared to the prediction of the harmonic approximation. The anharmonic contribution is close to 10%. Because of the flatness of the on-site potential in the directions parallel to the surface, the corresponding mean square displacements in these directions are much larger ($W_\parallel \approx 0.03\,\text{Å}^2$ at $T=0$), while the anharmonic contribution to this quantity does not exceed 6% in the temperature range between 0 K and 600 K.

C. Renormalized dispersion and multiphonon bound states

In our system, the intersite coupling is small in comparison to the on-site potential and may therefore be treated in perturbation theory. At lowest order, the wave functions of the ground state Ψ_0 and the first excited state of stretching character $\Psi_{s1,\mathbf{q}}$ have the respective forms

$$\Psi_0 = \prod_l \psi_0(\mathbf{u}(l)), \tag{8}$$

$$\Psi_{s1,\mathbf{q}} = \frac{1}{\sqrt{\mathcal{N}}} \sum_l e^{i\mathbf{q}\cdot\mathbf{R}(l)} \psi_{s1}(\mathbf{u}(l)) \prod_{l' \neq l} \psi_0(\mathbf{u}(l')), \tag{9}$$

where the index $s1$ stands for the quantum number $\overline{n}$ of the first excited state of the one-oscillator Hamiltonian having predominantly stretching character, the index 0 denotes the ground state, $\mathbf{R}(l)$ is the equilibrium position of hydrogen atom l, and $\mathcal{N}$ is the total number of unit cells. By evaluating numerically matrix elements

$$J_\alpha^{(\overline{m},\overline{n})} = \int \psi_{\overline{m}}(\mathbf{u}) u_\alpha \psi_{\overline{n}}(\mathbf{u})\, d^3u, \tag{10}$$

$$K_{\alpha\beta}^{(\overline{m},\overline{n})} = \int \psi_{\overline{m}}(\mathbf{u}) u_\alpha u_\beta \psi_{\overline{n}}(\mathbf{u})\, d^3u, \tag{11}$$

we obtain the frequencies $\omega_{\mathbf{q}s} = (\mathcal{E}_{s1,\mathbf{q}} - \mathcal{E}_0)/\hbar$ in first-order perturbation theory. In writing Eqs. (10) and (11), we have chosen the wave functions $\psi_{\overline{n}}$ to be real. The difference of the energies $\mathcal{E}_{s1,\mathbf{q}}$ and $\mathcal{E}_0$ associated with the wave functions $\Psi_{s1,\mathbf{q}}$ and Ψ_0 within this approximation is

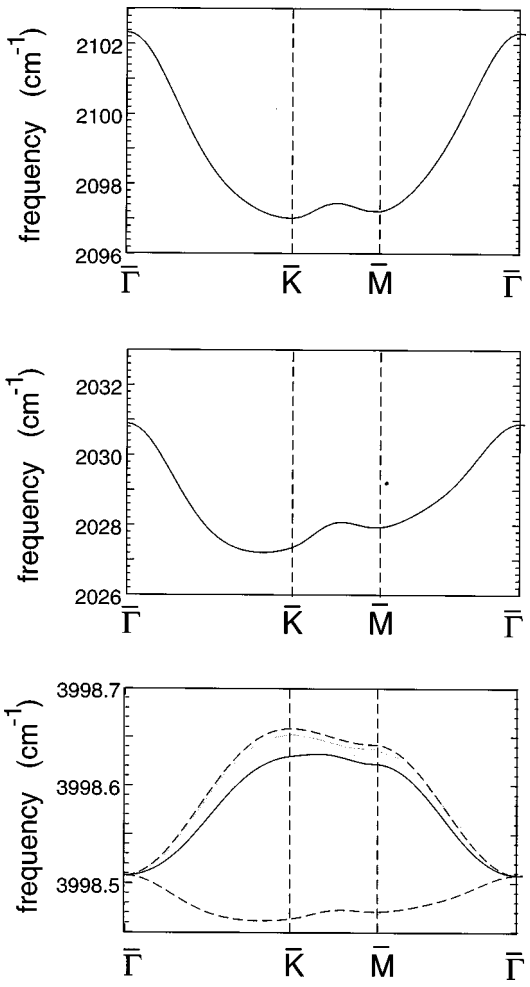

FIG. 10. Top and center, one-phonon dispersion curve of the hydrogen stretching mode within rigid substrate approximation. Top, harmonic approximation; center, with anharmonic on-site potential; bottom, Dispersion of the ''two-phonon bound state'' energy; thick solid, rigid-substrate Hamiltonian with full anharmonic on-site potential, first-order + second-order perturbation theory with respect to intersite coupling; lower dashed, contribution of first-order perturbation theory; thin solid, Bose-Hubbard model with parameters from *ab initio* frozen phonon calculations by Li and Vanderbilt (Ref. 23); upper dashed, Bose-Hubbard model of Li and Vanderbilt, second-order perturbation theory with respect to hopping parameter. All curves shifted to the same frequency value at the $\bar{\Gamma}$ point.

$$\mathcal{E}_{s1,\mathbf{q}}-\mathcal{E}_0=E_{s1}-E_0+\frac{1}{2}\sum_{l\neq 0}\phi_{\alpha\beta}(l0)\times[2\cos(\mathbf{q}\cdot\mathbf{R}(l))J_\alpha^{(s1,0)}J_\beta^{(s1,0)}+J_\alpha^{(s1,s1)}J_\beta^{(0,0)}+J_\alpha^{(0,0)}J_\beta^{(s1,s1)}-2J_\alpha^{(0,0)}J_\beta^{(0,0)}-K_{\alpha\beta}^{(s1,s1)}+K_{\alpha\beta}^{(0,0)}]. \tag{12}$$

Here, E_0 and E_{s1} are the ground state energy and energy value of the first excited state of predominantly stretching character of a single oscillator with no intersite coupling. The quantities $\hbar\omega_{\mathbf{qs}}$, which may be regarded as vibronic quasiparticle energies of the anharmonic system, are displayed in Fig. 10 and compared to the harmonic phonon frequencies as obtained by diagonalizing the dynamical matrix. Apart from the shift of $71\,\mathrm{cm}^{-1}$, the two dispersion curves also differ by their bandwidths and partly their shapes.

In the same way as for the energies $\mathcal{E}_{s1,\mathbf{q}}$ one may use perturbation theory to calculate higher vibrational energies of our system of weakly coupled anharmonic oscillators. Due to lattice translational invariance, these energies can be characterized by a wave vector **q**, and the corresponding wavefunctions have Bloch form. In addition to wave functions of the form (9) which is a linear combination of states with one oscillator in an excited state while all the others being in the ground state (states of type I), there are also those with two and more oscillators being in excited states (states of type II), which have to be taken into account as zero-order wave functions in the perturbation calculation. In the case of harmonic oscillators, the states of type I are degenerate with those of type II, and for a given Bloch wave vector **q**, continuous bands of energies arise. In the case of strongly anharmonic oscillators, the zero-order energy of a state of type I, $(\mathcal{E}_0+E_n^-E_0)$, may differ from the zero-order energy of any state of type II ($\mathcal{E}_0$ plus a sum of integer multiples of one-oscillator excitation energies $E_n^-E_0$) by much more than the intersite interaction matrix elements. In this case, it is obvious that the energy spectrum of the coupled many-oscillator system for given wave vector **q** contains, in addition to continuous bands, isolated points corresponding to states which are predominantly of type I, i.e., one oscillator is in an excited state while the others are in their ground state. These correspond to the *N*-phonon bound states. Two-phonon bound states have first been considered for bulk crystals in the late sixties.[54,55] Later, it has been recognized that they are likely to occur in adsorbate systems,[56,57] and in the meantime, they have been found and investigated experimentally and theoretically for Si(111):H,[15,23] C(111):H,[58] and Ru(001):CO.[59,60] Because of the complex structure of the single-oscillator spectrum, the condition that the zero-order energy of states of type I is sufficiently different from any zero-order energy of states of type II can be met only for low energy levels. We consider here the state of type I with one oscillator being in the second excited state of predominantly stretching character (which corresponds to the 23rd single-oscillator level). We denote this level by $s2$. The state of type II coming closest to it in energy has seven oscillators in the first excited state of predominantly bending character. The energy difference is $13.4\,\mathrm{cm}^{-1}$, which is still considerably larger than the bandwidth of the stretching mode due to the intersite interaction, but of the same order of magnitude as the bandwidth of the bending modes. However, coupling between these two states occurs only in high-order perturbation theory and may therefore be neglected. Consequently, there is a single branch separated from the continuous bands in the energy spectrum of the many-oscillator system. We calculate the dispersion $\mathcal{E}_{s2,\mathbf{q}}$ of this branch using perturbation theory up to second order. The first-order contribution is of the form (12) with $s1$ replaced by $s2$. It is very small since the matrix elements $J_\alpha^{(s2,0)}$ are small. (They would vanish in the case of harmonic oscillators). In second order of the intersite interaction, we take into account only the dominant contribution, which is the coupling to states of type II with two oscillators being in the first excited state of pre-

dominantly stretching character $(s1)$, while the other oscillators are in their ground state. It has the explicit form

$$\Delta_2\mathcal{E}_{s2,\mathbf{q}}=\frac{|J_3^{(s1,s2)}J_3^{(s1,0)}|^2}{E_0+E_{s2}-2E_{s1}}\sum_{l\neq 0}\phi_{33}^2(0l)\{1+\cos[\mathbf{q}\cdot\mathbf{R}(l)]\}. \tag{13}$$

Figure 10(c) shows the dispersion of the ''two-phonon bound state'' which is extremely weak if compared even to the one-phonon dispersion of the stretching modes. The dispersion results mainly from the coupling to states of type II treated in second-order perturbation theory, but the first-order contribution is not negligible. However, the small silicon displacements accompanied by the displacements of the hydrogen atoms and neglected in the rigid substrate approximation may in fact have a larger effect on the dispersion of the ''two-phonon bound state'' than the intersite coupling in the Hamiltonian (1).

In Fig. 10(c) our results are also compared to an earlier, pioneering calculation of the dispersion of the ''two-phonon bound state'' by Li and Vanderbilt[23] on the basis of an *ad hoc* Ansatz for an effective Hamiltonian, namely, the boson Hubbard Hamiltonian

$$H_{\text{eff}}=\varepsilon_0\sum_l a_l^+a_l+\Gamma\sum_l (a_l^+)^2(a_l)^2+t\sum_{\langle ll'\rangle} a_l^+a_{l'}. \tag{14}$$

Here, a_l^+ and a_l are creation and annihilation operators. The last sum is running over nearest-neighbor pairs. The three parameters occurring in this Hamiltonian were obtained from frozen-phonon calculations. In particular, the relations $\varepsilon_0=E_{s1}-E_0$ and $2\Gamma=E_{s2}+E_0-2E_{s1}$ were used and the energies E_n^- of the on-site Hamiltonian were calculated by using an expansion of the on-site potential V in powers of the displacement components truncated after the fourth order,

$$V(\mathbf{u})=\tfrac{1}{2}m_H[\omega_b^2(u_1^2+u_2^2)+\omega_s^2u_3^2]+a_3u_3^3+b_3(u_1^2+u_2^2)u_3 +a_4u_3^4+b_4(u_1^2+u_2^2)u_3^2+c_4(u_1^2+u_2^2)^2. \tag{15}$$

The numerical determination of the lowest eigenvalues E_n^- for this Hamiltonian is affected by the complication that the potential is unstable for certain directions of $\mathbf{u}$. As the hopping parameter t is much smaller than the anharmonicity parameter Γ, second-order perturbation theory describes accurately the dispersion of the ''two-phonon bound state'' as demonstrated in Fig. 10(c). Unlike the treatment of the full Hamiltonian in the rigid substrate approximation, there is no contribution of first-order perturbation theory. A boson Hubbard Hamiltonian has also been applied to the infrared properties of the system Si(111):H-(1×1) by Persson.[62]

A straightforward derivation of an effective Hamiltonian of the form (14) from the original Hamiltonian (1) seems to be possible only in the regime of weak anharmonicity. Following Refs. 61 and 63 one may carry out a unitary transformation in the form of an expansion in powers of a small parameter η, which may be chosen as the ratio of the root mean square displacements due to zero-point motion and a length that is a typical ratio of force constants of nth and $(n+1)$th order, e.g., $|a_3/a_4|$. We use the expansion (15) in the rigid substrate Hamiltonian (1) and decompose the latter as

$$H_{RS}=H_2+\eta H_3+\eta^2H_4, \tag{16}$$

where H_2 represents the harmonic on-site part of H_{RS}, ηH_3 stands for the cubic anharmonic part of Eq. (15), and η^2H_4 consists of the quartic anharmonic part and of the intersite interaction. Starting from a unitary operator $S=1+i\eta A+\eta^2B+O(\eta^3)$ and choosing the operators A and B appropriately, the transformed Hamiltonian $\tilde{H}=S^{-1}H_{RS}S$ does not contain any terms of first order in η, and the second-order terms all commute with the number operators and are of the form

$$\Delta\tilde{H}=\frac{\hbar^2}{4}\sum_l\left\{\frac{N_1}{2\omega_s^2}(a_l^+)^2(a_l)^2 +\frac{N_2}{\omega_s\omega_b}a_l^+a_l[b_l^+b_l+c_l^+c_l] +\frac{M_1}{2\omega_b^2}[(b_l^+)^2(b_l)^2+(c_l^+)^2(c_l)^2]+\frac{M_2}{\omega_b^2}b_l^+b_lc_l^+c_l\right\} +\frac{\hbar}{2\omega_s}\sum_{l,l'}\phi_{33}(ll')a_l^+a_{l'}+\frac{\hbar}{2\omega_b}\sum_{l,l'}\{\phi_{11}(ll')b_l^+b_{l'} +\phi_{22}(ll')b_l^+b_{l'}+\phi_{12}(ll')[b_l^+c_{l'}+c_{l'}^+b_l]\}. \tag{17}$$

The coefficients in Eq. (17) are related to the coefficients in the expansion of the on-site potential (15) via

$$N_1=12a_4-30(a_3/\omega_s)^2, \tag{18}$$

$$N_2=4b_4-12\frac{a_3b_3}{\omega_s^2}+(2b_3)^2\left\{\frac{1}{(\omega_s+\omega_b)^2-\omega_b^2} +\frac{1}{(\omega_s-\omega_b)^2-\omega_b^2}\right\}, \tag{19}$$

$$M_1=12c_4-(2b_3/\omega_s)^2, \tag{20}$$

$$M_2=M_1-4c_4. \tag{21}$$

This effective Hamiltonian may also be obtained in a different way, that highlights the underlying physical approximation. One may start with the classical equations of motion for the displacements $\mathbf{u}(l)$. Introducing a stretched time coordinate $\tau=\eta^2t$ and extracting the fast oscillations by expanding

$$u_3(l,t)=A_l(\tau)e^{-i\omega_st}+\eta\{\tfrac{1}{2}\alpha_l^{(0)}(\tau)+\alpha_l^{(2)}(\tau)e^{-2i\omega_st} +\alpha_l^{(b)}(\tau)e^{-2i\omega_bt}\}+\text{c.c.}+O(\eta^2), \tag{22}$$

$$u_1(l,t)=B_l(\tau)e^{-i\omega_bt}+\eta\{\beta_l^{(+)}(\tau)e^{-i(\omega_s+\omega_b)t} +\beta_l^{(-)}(\tau)e^{-i(\omega_s-\omega_b)t}\}+\text{c.c.}+O(\eta^2), \tag{23}$$

$$u_2(l,t)=C_l(\tau)e^{-i\omega_bt}+\cdots, \tag{24}$$

one is led to three nonlinearly coupled discrete nonlinear Schrödinger equations:

$$2i\omega_s \frac{\partial}{\partial \tau} A_l = \sum_{l'} \phi_{33}(ll') A_{l'} + N_1 |A_l|^2 A_l + N_2 (|B_l|^2 + |C_l|^2) A_l , \tag{25}$$

$$2i\omega_b \frac{\partial}{\partial \tau} B_l = \sum_{l'} [\phi_{11}(ll') B_{l'} + \phi_{12}(ll') C_{l'}] + [M_1 |B_l|^2 + M_2 |C_l|^2 + N_2 |A_l|^2] B_l . \tag{26}$$

The third equation is obtained from the second by interchanging B and C. Discrete nonlinear Schrödinger equations have been studied extensively in the literature.[34,64] In particular, stationary spatially localized solutions have been found.[34] It has been pointed out that multi-phonon bound states may be regarded as quantum signatures of such intrinsically localized modes.[61,65–67] For our system Si(111):H, intrinsic localized modes have been predicted on the basis of the original Hamiltonian H_{RS} with an on-site potential of the form (15).[68]

Canonical quantization of the coupled nonlinear Schrödinger equations (25),(26) yields directly the expressions of Eq. (17) for the anharmonic and intersite part of the Hamiltonian. Both ways of derivation of this Hamiltonian are based on the elimination of nonresonant couplings, while the resonant ones, which commute with the number operator, have been kept. The Hamiltonian (17) is obviously not the same as the one used by Li and Vanderbilt[23] as it contains explicitly the degrees of freedom associated with the bending motion. We will refer to this Hamiltonian in the next section.

The effect on the infrared absorption spectrum is the following: at zero temperature, the ''two-phonon bound state'' is visible as a sharp peak at frequency $(\mathcal{E}_{s2,\mathbf{0}} - \mathcal{E}_0)/\hbar$ with intensity proportional to $|J_3^{(0,s2)}|^2$, which vanishes in the harmonic approximation. The continuum of states of type II remains invisible at zero temperature. Only if ''one-phonon states'' of the type (9) are populated, these states will become visible. We note that due to the smallness of the second-order dipole moments in our system as found in Sec. IV A, a two-phonon continuum at $T=0$ K will not be exhibited by second-order infrared absorption, either.

In the case of the bending modes, the frequency shift due to zero-point motion and the bandwidth of the dispersion curve are of the same order of magnitude. Consequently, perturbation theory with respect to the intersite coupling cannot be done in the same way as for the stretching vibration described above.

V. COUPLING TO SUBSTRATE MODES

For a proper description of temperature effects on the infrared spectrum of our system, the coupling to substrate vibrational modes is paramount. In order to include the displacements of the silicon atoms in the theory, we extend our notation in the following way: l continues to label the elementary cell of the slab. In addition, we introduce a sublattice index κ. $\kappa=0$ stands for the hydrogen sublattice. When referring to the silicon sublattices, we use the index σ.

Because of their comparatively large atomic mass, the mean square displacements of the silicon atoms is much smaller than those of the hydrogen atoms and consequently, we may truncate the expansion of the lattice potential Φ in powers of the displacement components after the third order of the silicon displacements:

$$\begin{aligned}\Phi(\{\mathbf{u}(l\kappa)\}) = {} & \Phi_{RS}(\{\mathbf{u}(l0)\}) \\ & + \sum_{l,\sigma,\alpha} \Phi_\alpha^{(1)}(\{\mathbf{u}(l0)\}|l\sigma) u_\alpha(l\sigma) \\ & + \frac{1}{2} \sum_{l,\sigma,\alpha} \sum_{l',\sigma',\beta} \Phi_{\alpha\beta}^{(2)}(\{\mathbf{u}(l0)\}|l\sigma l'\sigma') \\ & \times u_\alpha(l\sigma) u_\beta(l'\sigma') \\ & + O(u(l\sigma)^3).\end{aligned} \tag{27}$$

Here, Φ_{RS} is the rigid substrate part of the potential that we have considered in the previous section. The quantities Φ_{RS}, $\Phi_\alpha^{(1)}(l\sigma)$, and $\Phi_{\alpha\beta}^{(2)}(l\sigma l'\sigma')$ are functions of the hydrogen displacements. To determine the latter two fully *ab initio* would go beyond our current numerical resources. Therefore, we have expanded the three functions in powers of the hydrogen displacements and have retained in Eq. (27) terms up to quartic anharmonicity. This may not always be adequate in view of the large mean square displacements of the hydrogen atoms. However, it has been found that on the basis of this approximation, results for the temperature dependence of the stretching mode frequency and linewidth can be gained that are in quite good agreement with experiment. Transforming to phonon normal coordinates $A(\mathbf{q}j)$ via

$$\mathbf{u}(l\kappa) = \sum_{\mathbf{q}j} e^{i\mathbf{q}\cdot\mathbf{R}(l)} \mathbf{e}(\kappa|\mathbf{q}j) \left(\frac{\hbar}{\mathcal{N} M_\kappa 2\omega_{\mathbf{q}j}} \right)^{1/2} A(\mathbf{q}j) \tag{28}$$

and the components $\epsilon_{\alpha\beta}$ of the deformation tensor accounting for homogeneous deformations, the lattice potential may be written in the form

$$\begin{aligned}\Phi = {} & \frac{\hbar}{4} \sum_{\mathbf{q}j} \omega_{\mathbf{q}j} A(\mathbf{q}j) A(-\mathbf{q}j) + \frac{1}{2} \sum_{\alpha,\beta,\mu,\nu} \epsilon_{\alpha\beta} S_{\alpha\beta\,\mu\nu} \epsilon_{\mu\nu} + \sum_{\alpha,\beta} \sum_j d_{\alpha\beta}(j) \epsilon_{\alpha\beta} A(\mathbf{0}j) \\ & + \frac{\hbar}{3!} \sum_{\mathbf{q}j,\mathbf{q}'j',\mathbf{q}''j''} V_3(\mathbf{q}j,\mathbf{q}'j',\mathbf{q}''j'') A(\mathbf{q}j) A(\mathbf{q}'j') A(\mathbf{q}''j'') + \frac{\hbar}{2} \sum_{\alpha\beta} \sum_{\mathbf{q}j,\mathbf{q}'j'} V_{\alpha\beta}(\mathbf{q}j,\mathbf{q}'j',-) A(\mathbf{q}j) A(\mathbf{q}'j') \epsilon_{\alpha\beta} \\ & + \cdots + \frac{\hbar}{4!} \sum_{\mathbf{q}j,\mathbf{q}'j'} \sum_{\mathbf{q}''j'',\mathbf{q}'''j'''} V_4(\mathbf{q}j,\mathbf{q}'j',\mathbf{q}''j'',\mathbf{q}'''j''') A(\mathbf{q}j) A(\mathbf{q}'j') A(\mathbf{q}''j'') A(\mathbf{q}'''j''') + \cdots .\end{aligned} \tag{29}$$

Here, $\mathbf{q}$ is the wave vector in the surface Brillouin zone, the index j labels the phonon branches, and $[\mathbf{e}(\kappa|\mathbf{q}j)]$ denotes the eigenvector associated with the phonon mode $(\mathbf{q}j)$. In Eq. (29), only those terms have been stated explicitly that occur in the perturbation-theoretical results discussed in the following subsections.

A. Temperature dependent equilibrium positions

Before considering the anharmonic effects on the frequency and linewidth of the hydrogen adsorbate vibrations, we first address the role of the zero-point motion and the thermal fluctuations of the atoms on the equilibrium positions as they turn out to have an important influence on the anharmonic frequency shift. The static equilibrium conditions are obtained from Eq. (29) by performing the derivatives of the potential energy with respect to the quantities $\epsilon_{\alpha\beta}$ and to the coordinates $A(\mathbf{0}j)$ and equating to zero the quantum-statistical averages of these derivatives. If we confine ourselves to lowest order in the anharmonicity, i.e., if we retain only those terms that give corrections of order $\hbar$ to the static displacements in the limit $T\rightarrow 0$, the following equations are obtained:

$$0=\frac{\hbar}{2}\omega_{\mathbf{0}j}\langle A(\mathbf{0}j)\rangle+\sum_{\alpha\beta} d_{\alpha\beta}(j)\epsilon_{\alpha\beta} + \frac{\hbar}{2}\sum_{\mathbf{q},j',j''} V_3(\mathbf{0}j,\mathbf{q}j',-\mathbf{q}j'')\langle A(\mathbf{q}j')A(-\mathbf{q}j'')\rangle_{\mathrm{o}}, \tag{30}$$

$$0=S_{\alpha\beta\,\mu\nu}\epsilon_{\mu\nu}+\sum_{j} d_{\alpha\beta}(j)\langle A(\mathbf{0}j)\rangle + \frac{\hbar}{2}\sum_{\mathbf{q},j',j''} V_{\alpha\beta}(\mathbf{q}j',-\mathbf{q}j'',-)\langle A(\mathbf{q}j')A(-\mathbf{q}j'')\rangle_{\mathrm{o}}. \tag{31}$$

The brackets $\langle\cdots\rangle$ stand for the quantum-statistical average and the index o indicates that this average has to be performed with the statistical operator that corresponds to the harmonic part of the Hamiltonian.

The variables occurring in Eqs. (30,31) are partly redundant since a homogeneous deformation of a finite slab with $\epsilon_{\alpha\beta}=\delta_{\alpha3}\delta_{\beta3}\epsilon_{33}$ can also be described by a superposition of normal displacements with wave vector $\mathbf{q}=\mathbf{0}$. With increasing size of the slab, the effect of the surfaces on the homogeneous deformation induced by zero-point motion and thermal fluctuations diminishes. The only possible homogeneous deformations of an infinite crystal consistent with the cubic symmetry of silicon are of the form $\epsilon_{\alpha\beta}=\delta_{\alpha\beta}\epsilon_0$. Therefore, we may replace Eq. (31) by the corresponding equation for bulk silicon,

$$B_0\epsilon_0=\frac{1}{6\Omega_0}\sum_{\mathbf{q},j}\gamma(\mathbf{q}j)\hbar\omega_{\mathbf{q}j}(2n_{\mathbf{q}j}+1), \tag{32}$$

where B_0 is the bulk modulus of silicon, Ω_0 is the crystal volume, $\gamma(\mathbf{q}j)$ is the Grüneisen constant of the bulk phonon mode $(\mathbf{q}j)$ and $n_{\mathbf{q}j}$ its Bose factor. *Ab initio* data for the Grüneisen constants of silicon are available[69] and have been used to calculate ϵ_0 as function of temperature. For practical reasons, mean sublattice displacement vectors $\mathbf{U}(\kappa)$ instead of the (quantum-thermally) averaged normal coordinates $\langle A(\mathbf{0}j)\rangle$ are used as variables in the calculations. In this way, our procedure of derivation becomes very similar to the one by Dobrzynski and Maradudin,[70] except that we expand around the classical equilibrium positions (i.e., around the equilibrium positions of the relaxed system) rather than around the ideal positions. The static displacements $\langle u_\alpha(l\kappa)\rangle$ may then be decomposed as

$$\langle u_\alpha(l\kappa)\rangle=\sum_\beta \epsilon_{\alpha\beta}R_\beta(l\kappa)+U_\alpha(\kappa). \tag{33}$$

Symmetry requires that the additional displacements $\mathbf{U}(\kappa)$ can only have a nonzero component normal to the surface, $U_\alpha(\kappa)=\delta_{\alpha3}U(\kappa)$. Equation (30) then takes the form

$$0=\sum_{\kappa'} G(\kappa\kappa')U(\kappa')+\sum_{\mathbf{q}j} F^{(0)}(\kappa|\mathbf{q}j)(2n_{\mathbf{q}j}+1) + F^{(1)}(\kappa)\epsilon_0. \tag{34}$$

The coefficients occurring in Eq. (34) have been determined *ab initio* in the following way.

Using density-functional perturbation theory, dynamical matrices with components $D_{\alpha\beta}(\kappa\kappa'|\mathbf{q})$ have been calculated for the atoms at their classical equilibrium positions (i.e., for the relaxed slab) as well as for reference configurations with layers displaced from their equilibrium positions in the direction normal to the surface. The coefficients $G(\kappa\kappa')$ are simply equal to the components $D_{33}(\kappa\kappa'|\mathbf{0})$ of the dynamical matrix at the center of the Brillouin zone, evaluated at the equilibrium configuration and multiplied by $\sqrt{M_\kappa M_{\kappa'}}$ with M_κ being the mass of an atom of sublattice κ. The coefficients $F^{(0)}(\kappa|\mathbf{q}j)$ are obtained by taking numerical derivatives of dynamical matrices with respect to layer displacements,

$$F^{(0)}(\kappa|\mathbf{q}j)=\frac{\hbar}{2\omega_{\mathbf{q}j}}\sum_{\alpha,\beta}\sum_{\kappa',\kappa''} e^*_\alpha(\kappa'|\mathbf{q}j) \times\left[\frac{\partial}{\partial U(\kappa)}D_{\alpha\beta}(\kappa'\kappa''|\mathbf{q})\right]_{U(\kappa)=0} e_\beta(\kappa''|\mathbf{q}j). \tag{35}$$

The quantities $F^{(1)}(\kappa)\epsilon_0$ are simply the derivatives of the Hellmann-Feynman forces with respect to a homogeneous dilatation of all bond lengths. Because of translational invariance, we may fix $U(\kappa)=0$ at the center of the slab. The static layer displacements $U(\kappa)$ may be expected to have non-negligible values only for the adsorbate layer and the first few substrate layers, where surface relaxation occurs. In our calculations, we have allowed $U(\kappa)$ to be nonzero only for the hydrogen layer and the top substrate layer. (For practical reasons, the derivatives in Eq. (35) have been carried out with respect to displacements of the first substrate layer and with respect to the amplitude of the hydrogen stretching mode rather than the displacement of the adsorbate layer.) The resulting behavior of the hydrogen-silicon distance and the layer spacing between the first two substrate layers as function of temperature is shown in Fig. 8. The inclusion of

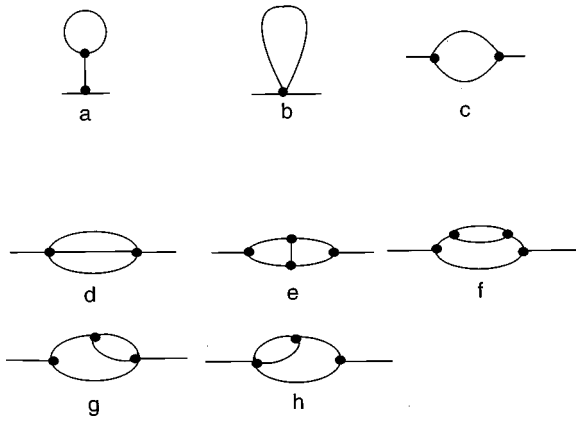

FIG. 11. Self-energy diagrams considered in the calculation of the anharmonic frequency shift and linewidth of the hydrogen stretching mode.

the coupling to the substrate modes modifies the behavior of the Si-H distance quantitatively, but does not alter the general tendency found in the rigid substrate approximation. On the other hand, the distance between the first two silicon layers monotonously increases with temperature, unlike the interatomic distances in the bulk which show a well-known minimum as function of temperature. The zero-point motion enlarges all distances as compared to their values corresponding to the classical equilibrium positions.

B. Anharmonic frequency shift

The anharmonic contribution to the frequency of the hydrogen stretching mode is calculated from the self-energy of this mode. There are three contributions to the phonon self-energy that are of first order in $\hbar$ at zero temperature. They are symbolized by the first three diagrams in Fig. 11. The sum of these three contributions may be arranged in the form

$$\Delta\omega_{\mathbf{0}s}=\sum_{\mathbf{q}j}\Omega(\mathbf{q}j)(2n_{\mathbf{q}j}+1) \tag{36}$$

with coefficients $\Omega=\Omega_L+\Omega_B+\Omega_T$ that do not depend on temperature. The contribution of the loop diagram to the coefficient Ω is

$$\Omega_L(\mathbf{q}j)=\tfrac{1}{2}V_4(\mathbf{0}s,\mathbf{0}s,\mathbf{q}j,-\mathbf{q}j). \tag{37}$$

The bubble diagram yields

$$\Omega_B(\mathbf{q}j)=-\sum_{j'}\tfrac{1}{2}|V_3(\mathbf{0}s,\mathbf{q}j,-\mathbf{q}j')|^2\times\left[\frac{\omega_{\mathbf{q}j}+\omega_{\mathbf{q}j'}}{(\omega_{\mathbf{q}j}+\omega_{\mathbf{q}j'})^2-\omega_{\mathbf{0}s}^2}+\frac{\omega_{\mathbf{q}j'}-\omega_{\mathbf{q}j}}{(\omega_{\mathbf{q}j'}-\omega_{\mathbf{q}j})^2-\omega_{\mathbf{0}s}^2}\right]. \tag{38}$$

The contribution of the ''tadpole diagram'' to the anharmonic frequency shift is given by

$$(\Delta\omega_{\mathbf{0}s})_T=\sum_{\kappa}\left[\frac{\partial\omega_{\mathbf{0}s}}{\partial U(\kappa)}\right]_{U(\kappa)=0}U(\kappa)+\left[\frac{\partial\omega_{\mathbf{0}s}}{\partial\epsilon_0}\right]_{\epsilon_0=0}\epsilon_0. \tag{39}$$

Inserting the solution of Eq. (34) for $U(\kappa)$ and the expression Eq. (32) for ϵ_0 in Eq. (39), the contribution of the tadpole diagram is easily arranged in the form (36). We emphasize that the sum in Eq. (36) is over all surface/adsorbate and bulk phonon modes.

Due to the very high value of the stretching-mode frequency, the denominator in Eq. (38) can never be zero. It may become small if one of the two branch indices j or j' refers to the hydrogen stretching mode and the other one to an acoustic mode for small $|\mathbf{q}|$. In this case, however, the coupling coefficients are very small and the contribution of this combination of modes turns out to be negligible.

The anharmonic coupling coefficients $V_3(\mathbf{0}s,\mathbf{q}j,-\mathbf{q}j')$ and $V_4(\mathbf{0}s,\mathbf{0}s,\mathbf{q}j,-\mathbf{q}j)$ have again been determined *ab initio* by combining density functional perturbation theory (DFPT) with the frozen phonon method. Using DFPT, dynamical matrices have been calculated for a grid of wave vectors $\mathbf{q}$ in the irreducible segment of the surface Brillouin zone for slabs with atoms at their classical equilibrium positions and for slabs with the displacement pattern of the zone-center hydrogen stretching mode frozen in with amplitude $A(\mathbf{0}s)$. We then obtain

$$V_3(\mathbf{0}s,\mathbf{q}j,-\mathbf{q}j')=\frac{1}{2\sqrt{\omega_{\mathbf{q}j}\omega_{\mathbf{q}j'}}}\sum_{\alpha,\beta}\sum_{\kappa,\kappa'}e_\alpha^*(\kappa|\mathbf{q}j')\times\left[\frac{\partial}{\partial A(\mathbf{0}s)}D_{\alpha\beta}(\kappa\kappa'|\mathbf{q})\right]_{A(\mathbf{0}s)=0}\times e_\beta(\kappa'|\mathbf{q}j) \tag{40}$$

from numerical derivatives of the dynamical matrices. To determine $V_4(\mathbf{0}s,\mathbf{0}s,\mathbf{q}j,-\mathbf{q}j)$, one has to set $j=j'$ in Eq. (40) and replace the first by the second derivative with respect to $A(\mathbf{0}s)$. To illustrate the quartic anharmonic coupling of the zone-center hydrogen stretching mode with the other phonon modes of the system, we display in Fig. 12 the quantity

$$\tilde{V}^{(4)}(\mathbf{q},\omega)=\sum_j V_4(\mathbf{0}s,\mathbf{0}s,\mathbf{q}j,-\mathbf{q}j)\times\epsilon/[\epsilon^2+(\omega-\omega_{\mathbf{q}j})^2] \tag{41}$$

for wave vectors $\mathbf{q}$ along the edges of the irreducible triangle of the surface Brillouin zone. The width ϵ has been chosen to be 2 cm^{-1}. A corresponding representation of the cubic anharmonic coupling constants $V_3(\mathbf{0}s,\mathbf{q}j,-\mathbf{q}j)$ looks very similar. As expected, the anharmonic coupling of the zone-center stretching mode is mainly to the modes of the stretching and bending branches. In addition, there are appreciable contributions from a branch near the upper edge of the bulk phonon spectrum having a relative content of vibrational am-

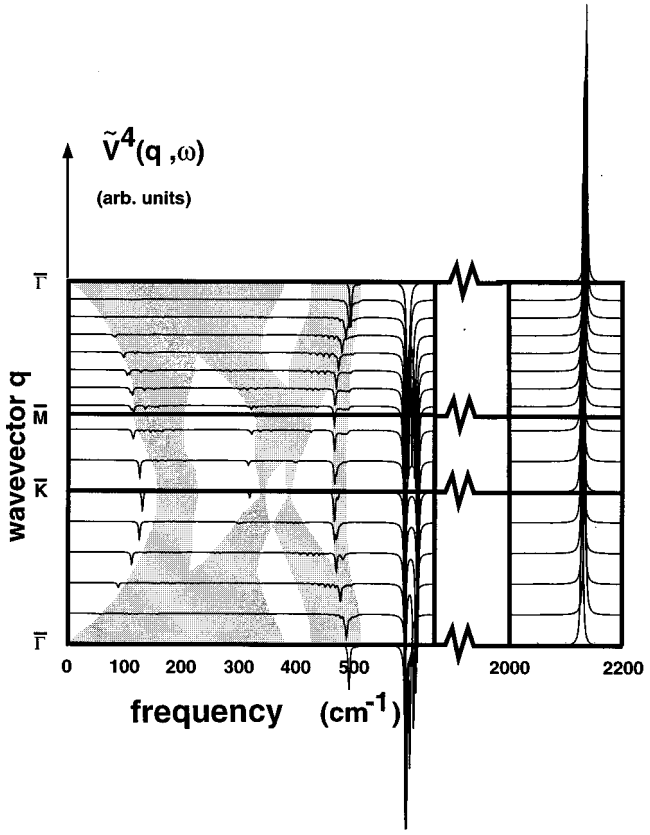

FIG. 12. Quartic anharmonic coupling coefficients. The function $\tilde{V}^{(4)}(\mathbf{q},\omega)$ is defined in the text.

plitudes of the hydrogen atoms higher than in other substrate modes (Lucas mode, see Sec. II). Coupling to the Rayleigh mode and another surface mode (S_6) can also be detected.

Inspired by theoretical work on adsorbate dynamics that was mainly focused on CO on metal surfaces,[71–73] earlier interpretations of experimental data on temperature dependent frequency and linewidth of the stretching mode[2] attributed the temperature dependence of these quantities to the anharmonic coupling of the stretching mode to a flat branch of surface phonons with a frequency of approximately $210\,\mathrm{cm}^{-1}$. Our *ab initio* calculations do in fact verify the existence of such a branch (see Fig. 3). However, as is apparent from Fig. 12, there is no anharmonic coupling of the zone-center stretching mode to this branch of surface phonons.

Evaluating the expressions (37), (38), and (39) with the anharmonic coupling coefficients determined *ab initio* in the way described above, we obtain results for the temperature dependence of the stretching mode frequency in quite good agreement with the experimental data, as shown in Fig. 13. These results are compared with those of an analogous calculation carried out within the rigid substrate approximation. This comparison clearly shows that at low temperatures, when the Bose factors for the bending modes become small, the substrate modes govern the temperature dependence. On the other hand, the contribution of the substrate modes to the anharmonic frequency shift at $T=0$ is negligible compared to that of the adsorbate modes.

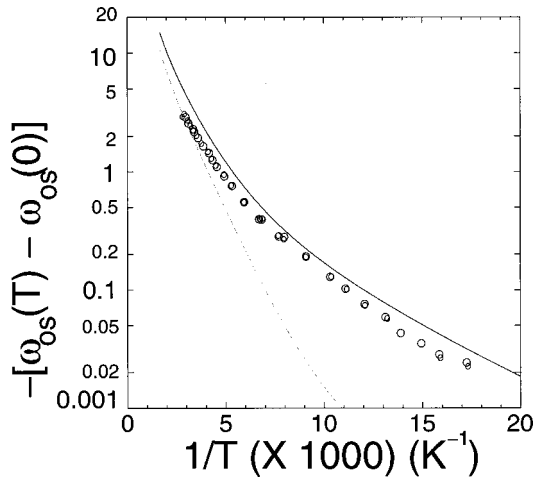

FIG. 13. Temperature-dependence of the stretching mode frequency. Solid, including coupling to substrate modes; dashed, without coupling to substrate modes; circles, IRAS data (this work).

Figure 14 shows the contribution of Figs. 11(a)–11(c) to the frequency shift of the stretching mode. They are found to be all of the same order of magnitude. They strongly differ from each other in their behavior as functions of temperature, and the contribution of the tadpole diagram even changes sign at higher temperatures. Apparently, the contributions of the loop and tadpole diagrams vary much more strongly with temperature than the total frequency shift. Neglecting one of the three contributions, would give a result that is not only quantitatively wrong, but also produces a qualitatively incorrect temperature dependence.

At zero temperature, all three contributions to the frequency of the stretching mode have the same sign. This is not the case for the bending mode. Here, strong compensations occur between the three different diagrams, which makes quantitative predictions very difficult.

Experimental information on the frequency shift due to zero-point motion can be gained through the isotope effect, i.e., by comparing the experimental frequencies for hydrogen and deuterium adsorbate atoms. In order to extract this information from the difference between the hydrogen and deuterium stretching frequencies (or bending frequencies), knowledge of the harmonic interplanar force constants between the first few layers is required. Harmonic frequencies for the system Si(111):D have been calculated by several authors.[19,74,75]

C. Intrinsic linewidth

The intrinsic width of the infrared absorption line at the stretching-mode frequency results from the imaginary part of the self-energy associated with this phonon mode. At zero temperature, a nonzero imaginary part arises from spontaneous decay. Because of the high value of the stretching mode frequency as compared to other phonon modes and the energy conservation condition, such decay processes require at least four phonon modes as decay products. Therefore, a nonzero imaginary part of the self-energy arises only at order

$\hbar^3$. However, at finite temperatures, scattering processes may occur that correspond to self-energy diagrams that are formally of order $\hbar^2$ at $T=0$. All diagrams of this sort that give a nonzero contribution to the imaginary part of the self-energy of the stretching mode are represented by Figs. 11(d)–11(h). Explicit expressions for the contributions of these diagrams are given in Ref. 76 [apart from (f) which may be easily evaluated following the rules given therein]). In the temperature range where the infrared absorption experiments have been carried out, the thermal occupation number of the stretching mode is negligibly small. We account for this fact and use the following simple Lorentzian form for the spectral functions $S_{\mathbf{q}j}(\omega)$ associated with the phonon lines occurring in these diagrams:

$$S_{\mathbf{q}j}(\omega)\approx 2(1+n_{\mathbf{q}j})\frac{\Gamma_{\mathbf{q}j}}{(\omega_{\mathbf{q}j}-\omega)^2+\Gamma_{\mathbf{q}j}^2} + 2n_{\mathbf{q}j}\frac{\Gamma_{\mathbf{q}j}}{(\omega_{\mathbf{q}j}+\omega)^2+\Gamma_{\mathbf{q}j}^2}. \tag{42}$$

Furthermore, we make use of the smallness of the damping constants $\Gamma_{\mathbf{q}j}$ in comparison with the mode frequencies $\omega_{\mathbf{q}j}$. The contributions of the diagrams represented in Figs. 11(d)–11(h) to the imaginary part $-\tilde{\Gamma}_{\mathbf{0}s}(\omega)$ of the self-energy at frequencies ω in the neighborhood of the frequency of the stretching mode $\omega_{\mathbf{0}s}$ may then be written in the compact form

$$\tilde{\Gamma}_{\mathbf{0}s}(\omega)=\pi\sum_{\mathbf{q},\mathbf{q}',\mathbf{q}''}\sum_{j',j''}|V_4^{\mathrm{eff}}(\mathbf{0}s,\mathbf{q}s,\mathbf{q}'j',\mathbf{q}''j'')|^2 n_{\mathbf{q}''j''}(1+n_{\mathbf{q}'j'})\frac{\Gamma_{\mathbf{q}s}+\Gamma_{\mathbf{q}'j'}+\Gamma_{\mathbf{q}''j''}}{(\omega-\omega_{\mathbf{q}s}-\omega_{\mathbf{q}'j'}+\omega_{\mathbf{q}''j''})^2+(\Gamma_{\mathbf{q}s}+\Gamma_{\mathbf{q}'j'}+\Gamma_{\mathbf{q}''j''})^2}. \tag{43}$$

(See also Burke *et al.*,[77] who use somewhat different arguments to arrive at an effective quartic vertex). The effective quartic anharmonic coupling coefficient consists of bare cubic and quartic coupling constants:

$$V_4^{\mathrm{eff}}(\lambda_1,\lambda_2,\lambda_3,\lambda_4)=V_4(\lambda_1,\lambda_2,\lambda_3,\lambda_4)-\sum_{\lambda_5}\left[V_3(\lambda_1,\lambda_4,\lambda_5)V_3(\lambda_2,\lambda_3,\overline{\lambda_5})\frac{2\omega_{\lambda_5}}{\omega_{\lambda_5}^2-(\omega_{\lambda_2}+\omega_{\lambda_3})^2}\right.$$
$$\left.+V_3(\lambda_1,\lambda_3,\lambda_5)V_3(\lambda_2,\lambda_4,\overline{\lambda_5})\frac{2\omega_{\lambda_5}}{\omega_{\lambda_5}^2-(\omega_{\lambda_2}-\omega_{\lambda_4})^2}+V_3(\lambda_1,\lambda_2,\lambda_5)V_3(\lambda_3,\lambda_4,\overline{\lambda_5})\frac{2\omega_{\lambda_5}}{\omega_{\lambda_5}^2-(\omega_{\lambda_3}-\omega_{\lambda_4})^2}\right]. \tag{44}$$

To simplify the notation, we have abbreviated $\mathbf{q}j$ by λ and $-\mathbf{q}j$ by $\overline{\lambda}$ in Eq. (44).

An *ab initio* calculation of all the anharmonic coupling coefficients occurring in Eq. (44) would be quite impossible at present. Instead, we resort to the following approximation. On the observation that the dominant anharmonic coupling of the stretching modes is to bending (b) and stretching (s) modes, we restrict the branch indices in Eqs. (43) and (44) to the adsorbate modes. Furthermore, we evaluate the effective quartic coupling coefficients within the rigid substrate approximation to obtain

$$V_4^{\mathrm{eff}}(\mathbf{0}s,\mathbf{q}s,\mathbf{q}'b,\mathbf{q}''b')=\frac{\hbar}{4\mathcal{N}m_H^3\omega_s\omega_b}N_2\Delta(\mathbf{q}+\mathbf{q}'+\mathbf{q}'')\times[\mathbf{e}(\mathbf{q}'b)\cdot\mathbf{e}(\mathbf{q}''b')]. \tag{45}$$

Here, $\mathcal{N}$ is again the number of unit cells. The coefficient N_2 is defined in Eq. (19), $\Delta(\cdots)$ is the Born-Huang δ function and $\mathbf{e}(\mathbf{q}b)$ is the eigenvector of the bending mode with wave vector $\mathbf{q}$ of branch (polarization index) b. We note that the same expression may be obtained in an alternative way when starting from the Hamiltonian (17), into which the anharmonic interaction with substrate modes may be included.

To evaluate the imaginary part (43) of the self-energy we make the additional assumption that the variation of the damping constants $\Gamma_{\mathbf{q}s}$ and $\Gamma_{\mathbf{q}b}$ with wave vector $\mathbf{q}$ is negligible. The sum of three damping constants on the right-hand side of Eq. (43) may then be replaced by $\Gamma_{\mathbf{0}s}+2\Gamma_{\mathbf{0}b}$. The intrinsic damping of the bending modes is predominantly due to decay into two substrate modes. The damping constant of the zone-center bending modes $\Gamma_{\mathbf{0}b}$ has therefore been calculated by using the formula

$$\Gamma_{\mathbf{0}b}=\frac{\pi}{2}\sum_{\mathbf{q}}\sum_{j,j'}|V_3(\mathbf{0}b,\mathbf{q}j,-\mathbf{q}j')|^2\times(1+n_{\mathbf{q}j}+n_{\mathbf{q}j'})\,\delta(\omega_{\mathbf{0}b}-\omega_{\mathbf{q}j}-\omega_{\mathbf{q}j'}), \tag{46}$$

where the branch indices j and j' refer to substrate modes only. The cubic anharmonic coupling coefficients $V_3(\mathbf{0}b,\mathbf{q}j,-\mathbf{q}j')$ have again been calculated *ab initio* by determining via density-functional perturbation theory dynamical matrices for a slab with a frozen-in displacement pattern of a zone-center bending mode with amplitude $A(\mathbf{0}b)$. The cubic coupling coefficient is then obtained by determining the numerical derivative with respect to $A(\mathbf{0}b)$ [according to Eq. (40) with s replaced by b]. The damping constant $\Gamma_{\mathbf{0}b}$ of the bending modes was found to vary between 2 and 8 cm^{-1} in the temperature range, 0–500 K (see Fig. 15).

Having calculated $\Gamma_{\mathbf{0}b}$ from Eq. (46), the damping constant $\Gamma_{\mathbf{0}s}$ of the stretching mode has then been determined self-consistently from the equation

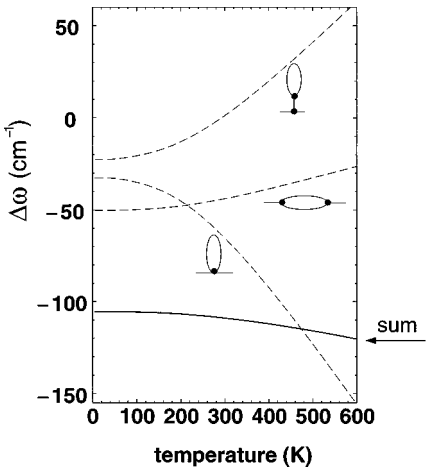

FIG. 14. Contributions to the anharmonic frequency shift of the three diagrams in Fig. 11 that are of first order in $\hbar$ at $T=0$.

$$\Gamma_{\mathbf{0}s}=\pi\left[\frac{\hbar \quad N_2}{4\mathcal{N}m_H^3\omega_s\omega_b}\right]^2 \times\sum_{\mathbf{q}',\mathbf{q}''}\sum_{b',b''}|\mathbf{e}(\mathbf{q}'b')\cdot\mathbf{e}(\mathbf{q}''b'')|^2 n_{\mathbf{q}''b''}(1+n_{\mathbf{q}'b'}) \times\frac{\Gamma_{\mathbf{0}s}+2\Gamma_{\mathbf{0}b}}{(\omega_{\mathbf{0}s}-\omega_{\mathbf{q}'+\mathbf{q}''s}-\omega_{\mathbf{q}'b'}+\omega_{\mathbf{q}''b''})^2+(\Gamma_{\mathbf{0}s}+2\Gamma_{\mathbf{0}b})^2}, \tag{47}$$

where summation indices b' and b'' run over the two bending mode branches. Equation (47) follows from Eq. (43), when identifying $\Gamma_{\mathbf{0}s}$ with $\tilde{\Gamma}_{\mathbf{0}s}(\omega_{\mathbf{0}s})$. This identification can be made, because the imaginary part of the self-energy as function of frequency ω varies little in the neighborhood of $\omega_{\mathbf{0}s}$ over a frequency range of the order of magnitude of $\tilde{\Gamma}_{\mathbf{0}s}(\omega_{\mathbf{0}s})$. This justifies the approximation of the spectral function for the stretching mode by a Lorentzian and thus the introduction of a damping constant for this mode. We emphasize that this would not be the case if the finite damping constants of the bending modes had not been taken into account.

Figure 15 compares the experimental data for the temperature dependence of the FWHM of the infrared absorption line with the theoretical results for $2\Gamma_{\mathbf{0}s}$ gained from Eq. (47). In the expression (19) for the coefficient N_2, strong compensations occur between the different terms. As a result, it is very sensitive to the values of the stretching and bending mode frequencies. When using the experimental values for ω_s and ω_b in the constant factor $[N_2/(\omega_s\omega_b)]^2$ of Eq. (47), good agreement can be achieved between theory and experiment. However, the theoretical linewidths would be much larger, if the bare (harmonic) frequencies were used. Figure 15 also shows that the temperature dependence of the damping constant for the bending modes is important for the correct description of the temperature dependence of $\Gamma_{\mathbf{0}s}$.

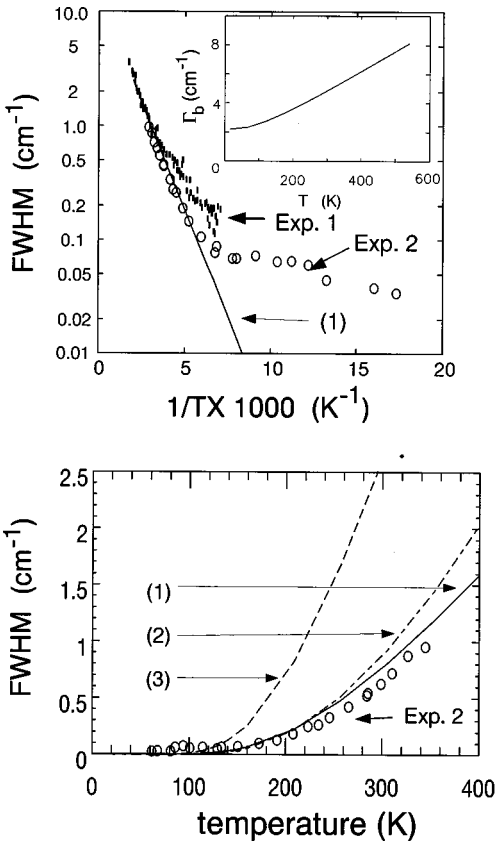

FIG. 15. Linewidth of the stretching mode as function of temperature. Experimental data (IRAS), Exp1, Ref. 2; Exp2, this work. Theory: (1) with Γ_b determined from two-phonon decay processes into substrate modes (right upper corner) and Γ_s determined self-consistently. In the effective quartic coupling constants, experimental values have been used for the stretching and bending mode frequencies. (2) same as (1) with $\Gamma_b=4\ \mathrm{cm}^{-1}=\mathrm{const}$. (3) same as (1) with harmonic frequencies used in the effective quartic coupling constants.

VI. CONCLUSION

The infrared absorption spectrum of the hydrogen-covered Si(111)(1×1) surface has been measured over a temperature range 14–350 K. A theoretical analysis has been given for the peak positions in the spectrum as well as for the temperature dependence of the position and linewidth of the main peak resulting from the nonlinear dynamics of the coupled system of adsorbate and substrate atoms. All quantities that govern this nonlinear dynamics have been determined *ab initio* by a plane-wave pseudopotential scheme based on the local-density approximation. Not only the electronic system, but also the anharmonic atomic vibrations have been treated fully quantum mechanically to properly describe the large quantum fluctuations of the hydrogen adsorbate atoms. In earlier work based on classical molecular-dynamics simulations, quantum fluctuations had been accounted for only to a certain degree of approximation by rescaling the temperature and depositing additional energy into the Si-H bonds[19] or by using Bloch-Redfield theory[78] which is limited to coupling between substrate and adsorbate degrees of freedom that is linear in the latter.

In our treatment of the problem, we have followed two routes that correspond to two different approximations. In the rigid-substrate approximation, we were able to treat the on-site anharmonicity of the hydrogen vibrations exactly and expand with respect to the weak intersite coupling. However, within this approximation, it is not possible to properly de-

scribe the measured temperature dependences of the stretching mode frequency and linewidth at low temperatures. Also, the rigid-substrate approximation ignores the presence of vibrational modes near the upper edge of the silicon bulk phonon spectrum that have an appreciable content of hydrogen motion.

When abandoning the rigid-substrate approximation and including the coupling to the vibrations of the substrate atoms, we had to retreat to perturbation theory valid for weak anharmonicity which may not give quantitatively reliable results in view of the large mean square displacements of the hydrogen atoms in their zero-point motion. Nevertheless, it has been possible within this approximation to obtain results for the temperature dependence of the stretching mode frequency and linewidth that are in quite good agreement with our experimental data. These data have been measured with an accuracy of a few percent of an inverse centimeter exceeding the accuracy of the corresponding theoretical values partly by orders of magnitude. A calculation of the stretching mode frequency that meets the precision of the experimental data in both the treatment of the electronic problem and the quantum and thermal fluctuations of the atomic positions remains a challenge for the theory.

ACKNOWLEDGMENTS

We are indebted to Dieter Strauch for a very helpful suggestion, and we would like to thank Matthias Scheffler and his group at the Fritz-Haber-Institut for having made available their *ab initio* molecular dynamics code. Financial support by the Deutsche Forschungsgemeinschaft (through Grants Nos. Ja524/1-1, Ja524/1-2, Ma1074/6, and Graduiertenkolleg ''Komplexität in Festkörpern: Phononen, Elektronen und Strukturen'') is gratefully acknowledged. We would also like to thank the HLRZ at the KFA Jülich (Project No. K2710000) and the Leibniz Rechenzentrum in Munich for granting us Cray computing time. A.P.M. thanks the MPIPKS Dresden for its kind hospitality.

*Present address: Physik-Department E20, Technische Universität München, D-85747 Garching, Germany.

[1] W. Mönch: *Semiconductor Surfaces and Interfaces*, 2nd ed. (Springer, Berlin, 1995).
[2] P. Dumas, Y. J. Chabal, and G. S. Higashi, Phys. Rev. Lett. **65**, 1124 (1990).
[3] G. S. Higashi, Y. J. Chabal, G. W. Trucks, and K. Raghavachari, Appl. Phys. Lett. **56**, 656 (1990).
[4] Y. J. Chabal, P. Dumas, P. Guyot-Sionnest, and G. S. Higashi, Surf. Sci. **242**, 524 (1991).
[5] E. Yablonovitch, D. L. Allara, C. C. Chang, T. Gmitter, and T. B. Bright, Phys. Rev. Lett. **57**, 249 (1986).
[6] E. T. Foley, A. F. Kam, J. W. Lyding, and Ph. Avouris, Phys. Rev. Lett. **80**, 1336 (1998).
[7] U. Harten, J. P. Toennies, Ch. Wöll, L. Miglio, P. Ruggerone, L. Colombo, and G. Benedek, Phys. Rev. B **38**, 3305 (1988).
[8] R. B. Doak, Y. J. Chabal, G. S. Higashi, and P. Dumas, J. Electron Spectrosc. Relat. Phenom. **54/55**, 291 (1990).
[9] Ch. Stuhlmann, G. Bogdányi, and H. Ibach, Phys. Rev. B **45**, 6786 (1992).
[10] P. Dumas and Y. J. Chabal, J. Vac. Sci. Technol. A **10**, 2160 (1992).
[11] P. Jakob and Y. J. Chabal, J. Chem. Phys. **95**, 2897 (1991).
[12] P. Jakob, Y. J. Chabal, Krishnan Raghavachari, and S. B. Christman, Phys. Rev. B **47**, 6839 (1993).
[13] Krishnan Raghavachari, P. Jakob, and Y. J. Chabal, Chem. Phys. Lett. **206**, 156 (1993).
[14] P. Guyot-Sionnest, Phys. Rev. Lett. **66**, 1489 (1991).
[15] P. Guyot-Sionnest, Phys. Rev. Lett. **67**, 2323 (1991).
[16] M. Morin, P. Jakob, N. J. Levinos, Y. J. Chabal, and A. L. Harris, J. Chem. Phys. **96**, 6203 (1992).
[17] K. Kuhnke, M. Morin, P. Jakob, N. J. Levinos, Y. J. Chabal, and A. L. Harris, J. Chem. Phys. **99**, 6114 (1993).
[18] W. Goldammer and W. Ludwig, Phys. Lett. A **133**, 85 (1988).
[19] B. J. Min, Y. H. Lee, C. Z. Wang, C. T. Chan, and K. M. Ho, Phys. Rev. B **46**, 9677 (1992).
[20] B. Sandfort, A. Mazur, and J. Pollmann, Phys. Rev. B **51**, 7139 (1995).
[21] J. A. Appelbaum and D. R. Hamann, Phys. Rev. Lett. **34**, 806 (1975).
[22] E. Kaxiras and D. Joannopoulos, Phys. Rev. B **37**, 8842 (1988).
[23] X.-P. Li and D. Vanderbilt, Phys. Rev. Lett. **69**, 2543 (1992).
[24] F. Ancilotto and A. Selloni, Phys. Rev. Lett. **68**, 2640 (1992).
[25] M. Buongiorno Nardelli, F. Finocchi, M. Palummo, R. Di Felice, C. M. Bertoni, F. Bernardini, and S. Ossicini, Surf. Sci. **270**, 879 (1992).
[26] H. Gai and G. A. Voth, J. Chem. Phys. **101**, 1734 (1994).
[27] R. Honke, P. Pavone, and U. Schröder, Surf. Sci. **367**, 75 (1996).
[28] J. Pollmann, A. Mazur, and P. Krüger (private Communication).
[29] P. Jakob, Y. J. Chabal, and K. Raghavachari, Chem. Phys. Lett. **187**, 325 (1991).
[30] P. Jakob, P. Dumas, and Y. J. Chabal, Appl. Phys. Lett. **59**, 2968 (1991).
[31] P. Guyot-Sionnest, P. Dumas, Y. J. Chabal, and G. S. Higashi, Phys. Rev. Lett. **64**, 2156 (1990).
[32] P. Guyot-Sionnest, P. Dumas, and Y. J. Chabal, J. Electron Spectrosc. Relat. Phenom. **54/55**, 27 (1990).
[33] A. J. Sievers and J. B. Page, in *Dynamical Properties of Solids VII*, edited by G. K. Horton and A. A. Maradudin (Elsevier, Amsterdam, 1995), p. 137.
[34] S. Flach and C. R. Willis, Phys. Rep. **295**, 181 (1998).
[35] W. Kern and D. A. Puotinen, RCA Rev. **31**, 187 (1970).
[36] W. Kern, Semicond. Int. **94** (1984).
[37] P. Jakob, Y. J. Chabal, K. Raghavachari, P. Dumas, and S. B. Christman, Surf. Sci. **295**, 251 (1993).
[38] A direct comparison of the dissimilar resonance frequencies in this work and in Ref. 2 is possible at room temperature. Our value of 2083.94 cm^{-1} is about 0.25 cm^{-1} higher than the one derived earlier (2083.7 cm^{-1}); therefore, the 0 K value given in Ref. 2 is too high by approximately 0.5 cm^{-1}.
[39] The deconvolution necessary to extract the linewidth at low temperatures requires a detailed knowledge of the instrumental lineshape and the inhomogeneous line shape. While the present system yields an extremely small inhomogeneous broadening its finite value ($\approx 0.05\ cm^{-1}$) is still an issue in accurately determining the homogeneous linewidth at low temperatures (data are available down to 14 K).
[40] The origin of this effect can be traced to water adsorption at low temperature. Deliberate exposure to water vapor (5 to 10 L at 90 K) were performed on a H/Si(111) surface held in an open

sample holder (no Cu shield in front). At low temperatures (<140 K), the Si-H stretch mode exhibits a 0.3 cm^{-1} redshift, with a corresponding broadening. Upon annealing, a marked narrowing and blueshift occurs at T>140 K, as the original spectrum of the water-free H/Si(111) surface is restored. Although a brief annealing could not be performed with the Cu sample holder used for the very low temperature experiments, this observation suggests that the anomalous shift at low T probably can be attributed to water physisorption on the H/Si(111) surface.

[41] J. Fritsch, P. Pavone, and U. Schröder, Phys. Rev. Lett. **71**, 4194 (1993).
[42] G. P. Kerker, J. Phys. C **13**, L189 (1980).
[43] N. Troullier and L. Martins, Phys. Rev. B **43**, 1993 (1991).
[44] S. Froyen, Phys. Rev. B **39**, 3168 (1989).
[45] S. Baroni, P. Giannozzi, and A. Testa, Phys. Rev. Lett. **58**, 1861 (1987).
[46] P. Giannozzi, S. de Gironcoli, P. Pavone, and S. Baroni, Phys. Rev. B **43**, 7231 (1991).
[47] M. Bockstedte, A. Kley, J. Neugebauer, and M. Scheffler, Comput. Phys. Commun. **107**, 187 (1997).
[48] D. R. Hamann, Bull. Am. Phys. Soc. **33**, 803 (1988).
[49] G. B. Bachelet, D. R. Hamann, and M. Schlüter, Phys. Rev. B **26**, 4199 (1982).
[50] D. R. Hamann, M. Schlüter, and C. Chiang, Phys. Rev. Lett. **43**, 1494 (1979).
[51] L. Kleinman and D. M. Bylander, Phys. Rev. Lett. **48**, 1425 (1982).
[52] Landolt-Börnstein, New Series, Group I, Vol. 2, edited by A. Eucken and K. H. Hellwege (Springer, Berlin, 1951).
[53] J. P. Perdew, J. A. Chevary, S. H. Vosko, K. A. Jackson, M. R. Pederson, D. J. Singh, and C. Fiolhais, Phys. Rev. B **46**, 6671 (1992).
[54] M. H. Cohen and J. Ruvalds, Phys. Rev. Lett. **23**, 1378 (1969).
[55] J. Ruvalds and A. Zawadowski, Phys. Rev. B **2**, 1172 (1970).
[56] A. G. Eguiluz and A. A. Maradudin, J. Electron Spectrosc. Relat. Phenom. **30**, 125 (1983).
[57] J. C. Ariyasu and D. L. Mills, Phys. Rev. B **28**, 2389 (1983).
[58] R. P. Chin, X. Blase, Y. R. Shen, and S. G. Louie, Europhys. Lett. **30**, 399 (1995).
[59] P. Jakob, Phys. Rev. Lett. **77**, 4229 (1996).
[60] P. Jakob and B. N. J. Persson, J. Chem. Phys. **109**, 8641 (1998).
[61] M. M. Bogdan and A. M. Kosevich, Fiz. Nizk. Temp. **2**, 794 (1976) [Sov. J. Low Temp. Phys. **2**, 391 (1976)].
[62] B. N. J. Persson, Phys. Rev. B **46**, 12 701 (1992).
[63] M. Wagner: *Unitary Transformations in Solid State Physics* (North-Holland, Amsterdam, 1986).
[64] J. C. Eilbeck, P. S. Lomdahl, and A. C. Scott, Physica D **16**, 318 (1985); for a bibliography see http://www.ma.hw.ac.uk/~chris/dst/
[65] A. C. Scott, J. C. Eilbeck, and H. Gilhøj, Physica D **78**, 194 (1994).
[66] W. Z. Wang, J. Tinka Gammel, A. R. Bishop, and M. I. Salkola, Phys. Rev. Lett. **76**, 3598 (1996).
[67] D. Bonart, Phys. Rev. B **56**, 244 (1997).
[68] U. Schröder, D. Bonart, and A. P. Mayer, Physica B **219&220**, 390 (1996).
[69] P. Pavone, Ph.D. dissertation, SISSA Trieste, 1991.
[70] L. Dobrzynski and A. A. Maradudin, Phys. Rev. B **7**, 1207 (1973).
[71] B. N. J. Persson and R. Ryberg, Phys. Rev. B **32**, 3586 (1985).
[72] B. N. J. Persson and R. Ryberg, Phys. Rev. B **40**, 10 273 (1989).
[73] D. C. Langreth and M. Persson, Phys. Rev. B **43**, 1353 (1991).
[74] V. Gräschus, A. Mazur, and J. Pollmann, Surf. Sci. **368**, 179 (1996).
[75] R. Honke, Ph.D. dissertation, Universität Regensburg, 1997.
[76] H. Bilz, D. Strauch, and R. K. Wehner, in *Vibrational Infrared and Raman Spectra of Nonmetals, Handbuch der Physik*, Vol. XXV/2d, edited by S. Flügge and L. Genzel (Springer, Berlin, 1984).
[77] K. Burke, D. C. Langreth, M. Persson, and Z.-Y. Zhang, Phys. Rev. B **47**, 15 869 (1993).
[78] H. Gai and G. A. Voth, J. Chem. Phys. **99**, 740 (1993).